Phylogenetic ctDNA analysis depicts early-stage lung cancer evolution

Abbosh, Christopher; Birkbak, Nicolai J; Wilson, Gareth A; Jamal-Hanjani, Mariam; Constantin, Tudor; Salari, Raheleh; Le Quesne, John; Moore, David A; Veeriah, Selvaraju; Rosenthal, Rachel; Marafioti, Teresa; Kirkizlar, Eser; Watkins, Thomas B K; McGranahan, Nicholas; Ward, Sophia; Martinson, Luke; Riley, Joan; Fraioli, Francesco; Al Bakir, Maise; Grönroos, Eva

DOI:
10.1038/nature22364

Phylogenetic ctDNA analysis depicts early stage lung cancer evolution

Christopher Abbosh[1*], Nicolai J. Birkbak[1,2*], Gareth A. Wilson[1,2*], Mariam Jamal-Hanjani[1*], Tudor Constantin[3*], Raheleh Salari[3*], John Le Quesne[4*], David A Moore[4+], Selvaraju Veeriah[1+], Rachel Rosenthal[1+], Teresa Marafioti[1,5], Eser Kirkizlar[3], Thomas B K Watkins[1,2], Nicholas McGranahan[1,2], Sophia Ward[1,2,6], Luke Martinson[4], Joan Riley[4], Francesco Fraioli[7], Maise Al Bakir[2], Eva Gronroos[2], Francisco Zambrana[1], Raymondo Endozo[7], Wenya Linda Bi[8,9], Fiona M. Fennessy[8,9], Nicole Sponer[3], Diana Johnson[1], Joanne Laycock[1], Seema Shafi[1], Justyna Czyzewska-Khan[1], Andrew Rowan[2], Tim Chambers[2,6], Nik Matthews[6,10], Samra Turajlic[2,11], Crispin Hiley1[2], Siow Ming Lee[12,1], Martin Forster[1,12], Tanya Ahmad[12], Mary Falzon[5], Elaine Borg[5], David Lawrence[13], Martin Hayward[13], Shyam Kolvekar[13], Nikolaos Panagiotopoulos[13], Sam M Janes[1,14,15], Ricky Thakrar[14], Asia Ahmed[16], Fiona Blackhall[17,18], Yvonne Summers[18], Dina Hafez[3], Ashwini Naik[3], Apratim Ganguly[3], Stephanie Kareht[3], Rajesh Shah[19], Leena Joseph[20], Anne Marie Quinn[20], Phil Crosbie[21], Babu Naidu[22], Gary Middleton[23], Gerald Langman[24], Simon Trotter[24], Marianne Nicolson[25], Hardy Remmen[26], Keith Kerr[27], Mahendran Chetty[28], Lesley Gomersall[29], Dean Fennell[4], Apostolos Nakas[30], Sridhar Rathinam[30], Girija Anand[31], Sajid Khan[32,33], Peter Russell[34], Veni Ezhil[35], Babikir Ismail[36], Melanie Irvin-sellers[37], Vineet Prakash[38], Jason Lester[39], Malgorzata Kornaszewska[40], Richard Attanoos[41], Haydn Adams[42], Helen Davies[43], Dahmane Oukrif[1], Ayse U Akarca[1], John A Hartley[44], Helen L Lowe[44], Sara Lock[45], Natasha Iles[46], Harriet Bell[46], Yenting Ngai[46], Greg Elgar[2,6], Zoltan Szallasi[47,48,49], Roland F Schwarz[50], Javier Herrero[51], Aengus Stewart[52], Sergio A Quezada[53], Peter Van Loo[54,55], Caroline Dive[56], Jimmy Lin[3], Matthew Rabinowitz[3], Hugo JWL Aerts[8,9,57], Allan Hackshaw[45], Jacqui A Shaw[4], Bernhard G. Zimmermann[3], and Charles Swanton[1,2] on behalf of the TRACERx and PEACE consortia.

*These authors contributed equally to this work +These authors contributed equally to this work

1. Cancer Research UK Lung Cancer Centre of Excellence, University College London Cancer Institute, Paul O'Gorman Building, 72 Huntley Street, London, WC1E 6BT
2. Translational Cancer Therapeutics Laboratory, The Francis Crick Institute, 1 Midland Rd, London NW1 1AT
3. Natera Inc., 201 Industrial Rd., San Carlos, United States, CA 94070
4. Cancer Studies, University of Leicester, Leicester, United Kingdom, LE2 7LX
5. Department of Pathology, University College London Hospitals, 235 Euston Rd, Fitzrovia, London, United Kingdom, NW1 2BU
6. Advanced Sequencing Facility, The Francis Crick Institute, 1 Midland Rd, London NW1 1AT
7. Department of Nuclear Medicine, University College London Hospitals, 235 Euston Rd, Fitzrovia, London, United Kingdom, NW1 2BU
8. Brigham and Women's Hospital, Boston, MA 02115, USA
9. Harvard Medical School, Boston, MA 02115, USA
10. Tumour Profiling Unit Genomics Facility, The Institute of Cancer Research, 237 Fulham Road, London, SW3 6JB
11. Renal and Skin Units, The Royal Marsden Hospital, London, SW3 6JJ
12. Department of Oncology, University College London Hospitals, 235 Euston Rd, Fitzrovia, London, United Kingdom, NW1 2BU
13. Department of Cardiothoracic Surgery, University College London Hospitals, 235 Euston Rd, Fitzrovia, London, United Kingdom, NW1 2BU
14. Department of Respiratory Medicine, University College London Hospitals, 235 Euston Rd, Fitzrovia, London, United Kingdom, NW1 2BU
15. Lungs for Living Research Centre. Division of Medicine, Rayne Building. University College London, 5 University Street. London. WC1E 6JF

16. Department of Radiology, University College London Hospitals, 235 Euston Rd, Fitzrovia, London, United Kingdom, NW1 2BU
17. Institute of Cancer Studies, University of Manchester, Oxford Road, Manchester, M13 9PL
18. The Christie Hospital, Manchester, United Kingdom, M20 4BX
19. Department of Cardiothoracic Surgery, University Hospitals of South Manchester, Manchester, M23 9LT
20. Department of Pathology, University Hospitals of South Manchester, Manchester, M23 9LT
21. North West Lung Centre, University Hospital of South Manchester, Manchester, United Kingdom, M23 9LT
22. Department of Thoracic Surgery, Birmingham Heartlands Hospital, Birmingham, United Kingdom, B9 5SS
23. Department of Medical Oncology, Birmingham Heartlands Hospital, Birmingham, United Kingdom, B9 5SS
24. Department of Cellular Pathology, Birmingham Heartlands Hospital, Birmingham, United Kingdom, B9 5SS
25. Department of Medical Oncology, Aberdeen University Medical School & Aberdeen Royal Infirmary, Aberdeen, Scotland, United Kingdom, AB25 2ZN
26. Department of Cardiothoracic Surgery, Aberdeen University Medical School & Aberdeen Royal Infirmary, Aberdeen, United Kingdom, AB25 2ZD
27. Department of Pathology, Aberdeen University Medical School & Aberdeen Royal Infirmary, Aberdeen, Scotland, United Kingdom, AB25 2ZD
28. Department of Respiratory Medicine, Aberdeen University Medical School & Aberdeen Royal Infirmary, Aberdeen, United Kingdom, AB25 2ZN

29. Department of Radiology, Aberdeen University Medical School & Aberdeen Royal Infirmary, Aberdeen, Scotland, United Kingdom, AB25 2ZN
30. Department of Thoracic Surgery, Glenfield Hospital, Leicester, LE3 9QP
31. Department of Radiotherapy, North Middlesex University Hospital, London N18 1QX
32. Department of Respiratory Medicine, Royal Free Hospital, Pond Street, London, NW3 2QG
33. Department of Respiratory Medicine, Barnet and Chase Farm Hospitals, Wellhouse Lane, Barnet, United Kingdom, EN5 3DJ
34. Department of Respiratory Medicine, The Princess Alexandra Hospital, Hamstel Rd, Harlow CM20 1QX
35. Department of Clinical Oncology, St.Luke's Cancer Centre, Royal Surrey County Hospital, Guildford, GU2 7XX
36. Department of Pathology, Ashford and St. Peters' Hospital, Guildford Road, Chertsey, Surrey, KT16 0PZ
37. Department of Respiratory Medicine, Ashford and St. Peters' Hospital, Guildford Road, Chertsey, Surrey, KT16 0PZ
38. Department of Radiology, Ashford and St. Peters' Hospital, Guildford Road, Chertsey, Surrey, KT16 0PZ
39. Department of Clinical Oncology, Velindre Hospital, Cardiff, Wales, United Kingdom, CF14 2TL
40. Department of Cardiothoracic Surgery, University Hospital Llandough, Cardiff, Wales, United Kingdom, CF64 2XX
41. Department of Cellular Pathology, University Hospital of Wales and Cardiff University, Heath Park Cardiff, Wales U.K

42. Department of Radiology, University Hospital Llandough, Cardiff, Wales, United Kingdom, CF64 2XX
43. Department of Respiratory Medicine, University Hospital Llandough, Cardiff, Wales, United Kingdom, CF64 2XX
44. UCL ECMC GCLP Facility, University College London Cancer Institute, Paul O'Gorman Building, 72 Huntley Street, London, WC1E 6BT
45. Department of Respiratory Medicine, The Whittington Hospital NHS Trust, United Kingdom, N19 5NF
46. University College London, Cancer Research UK & UCL Cancer Trials Centre, London, United Kingdom, W1T 4TJ
47. Centre for Biological Sequence Analysis, Department of Systems Biology, Technical University of Denmark, 2800 Lyngby, Denmark.
48. Computational Health Informatics Program (CHIP), Boston Children's Hospital, Harvard Medical School, Boston, MA, USA.
49. MTA-SE-NAP, Brain Metastasis Research Group, 2nd Department of Pathology, Semmelweis University, 1091 Budapest, Hungary.
50. Berlin Institute for Medical Systems Biology, Max Delbrueck Center for Molecular Medicine, Berlin, Germany
51. Bill Lyons Informatics Centre, University College London Cancer Institute, Paul O'Gorman Building, 72 Huntley Street, London, WC1E 6BT
52. Department of Bioinformatics and Biostatistics, The Francis Crick Institute, 1 Midland Rd, London NW1 1AT
53. Cancer Immunology Unit, University College London Cancer Institute, Paul O'Gorman Building, 72 Huntley Street, London, WC1E 6BT

54. Cancer Genomics Laboratory, The Francis Crick Institute, 1 Midland Rd, London NW1 1AT
55. Department of Human Genetics, University of Leuven, B-3000 Leuven, Belgium
56. Cancer Research UK Manchester Institute, Manchester, United Kingdom, M20 4BX
57. Dana-Farber Cancer Institute, 450 Brookline Ave. Boston, United States, MA 02215-5450

Corresponding author:

Charles Swanton

Translational Cancer Therapeutics Laboratory

The Francis Crick Institute

3rd Floor South West

1 Midland Road

London

NW1 1A

Email: Charles.Swanton@crick.ac.uk

Office +44 203 796 2047

Summary

The early detection of relapse following primary surgery for non-small cell lung cancer and the characterization of emerging subclones seeding metastatic sites might offer new therapeutic approaches to limit tumor recurrence. The potential to non-invasively track tumor evolutionary dynamics in ctDNA of early-stage lung cancer is not established. Here we conduct a tumour-specific phylogenetic approach to ctDNA profiling in the first 100 TRACERx (**TRA**cking non-small cell lung **C**ancer **E**volution through therapy (**Rx**)) study participants, including one patient co-recruited to the PEACE (**P**osthumous **E**valuation of **A**dvanced **C**ancer **E**nvironment) post-mortem study. We identify independent predictors of ctDNA release and perform tumor volume limit of detection analyses. Through blinded profiling of post-operative plasma, we observe evidence of adjuvant chemotherapy resistance and identify patients destined to experience recurrence of their lung cancer. Finally, we show that phylogenetic ctDNA profiling tracks the subclonal nature of lung cancer relapse and metastases, providing a new approach for ctDNA driven therapeutic studies

155 **Main text**

156 Lung cancer is the leading cause of cancer death[1-2]. Metastatic non-small cell lung cancer
157 (NSCLC) cannot be cured with systemic chemotherapy, yet clinical studies have shown a 5%
158 benefit of post-operative (adjuvant) chemotherapy on overall survival[3]. This modest survival
159 benefit may reflect a vulnerability of low volume disease within the context of reduced intra-
160 tumor heterogeneity[4]. Circulating tumor DNA (ctDNA) detection in plasma following
161 resection of breast[5,6] and colorectal[7] tumors has been shown to identify patients destined to
162 relapse post-operatively in advance of established clinical parameters. Identifying, monitoring
163 and genomically characterizing residual disease following primary lung cancer surgery may
164 improve outcomes in the adjuvant setting. This would create a therapeutic setting where only
165 patients destined to recur would receive treatment and where intervention could be directed to
166 the evolving tumor subclone that is seeding metastatic recurrence.

167 Here, we report a bespoke multiplex-PCR NGS approach to ctDNA profiling within the context
168 of the prospective tumor evolutionary NSCLC TRACERx study. We address determinants of
169 ctDNA detection in early-stage NSCLC and investigate the ability of ctDNA to identify and

genomically characterize post-operative NSCLC relapse within a tumor phylogenetic framework.

Phylogenetic ctDNA profiling

The TRACERx study monitors the clonal evolution of NSCLC from diagnosis through to death[8,9]. Using multi-region exome sequencing (M-Seq) derived tumor phylogenetic trees developed through prospective analysis of a 100 patient TRACERx cohort, we conducted a phylogenetic approach to ctDNA profiling in early-stage NSCLC **(Fig. 1).** Bespoke multiplex-PCR assay-panels were synthesised for each patient, targeting clonal and subclonal single nucleotide variants (SNVs) selected to track phylogenetic tumor branches in plasma **(Fig. 1)**. SNV detection in plasma was established through a calling algorithm employing negative control samples (see **Methods**). Analytical validation of the multiplex-PCR NGS platform demonstrated a sensitivity of above 99% for the detection of SNVs at frequencies above 0.1% and the specificity of detecting a single SNV was 99.6% (**Extended Data Fig. 1a**). At least two SNVs were detected in ctDNA from early-stage NSCLCs analyzed in our published discovery cohort data[10], demonstrating biological sensitivity of a two SNV threshold for ctDNA detection. Therefore, we prospectively selected a threshold of two detected SNVs for

calling a sample ctDNA positive for validation within this study; to minimize type I error when testing up to 30 tumour-specific SNVs per time-point in a single patient (see **Extended Data Fig. 1b** for justification).

Determinants of ctDNA detection in NSCLC

We sought to identify clinicopathological determinants of ctDNA detection in early-stage NSCLC by profiling pre-operative plasma samples in 100 TRACERx patients. Samples from four patients could not be analyzed (see cohort design **Extended Data Fig. 2a**, patient characteristics **Extended Table 1a-c, Supplementary Table 1**). Individual assay-panels were designed to target a median of 18 SNVs (range 10 to 22) comprising a median of 11 clonal SNVs (range 2 to 20) and a median of 6 subclonal SNVs (range 0 to 16) per patient **(Extended Data Fig. 2b,e)**.

At least two SNVs were detected in ctDNA pre-operatively in 46 of 96 (48%) early-stage NSCLCs and a single SNV was detected in 12 additional cases **(Fig. 2a)**. Centrally reviewed pathological data revealed that ctDNA detection was associated with histological subtype: 97% (30/31) of lung squamous cell carcinomas (LUSCs) and 71% (5 of 7) of other NSCLC subtypes were ctDNA positive, compared with 19% (11/58) of lung adenocarcinomas (LUADs) (**Fig.**

2a). 94% (16 of 17) of stage I LUSCs were detected compared with 13% (5 of 39) of stage I LUADs (**Extended Data Fig. 3a**). Passive release of ctDNA into the circulation may be associated with necrosis[11]. As expected LUSCs were significantly more necrotic than LUADs[12] and ctDNA positive LUADs formed a sub-group of more necrotic tumors compared with ctDNA negative LUADs **(Extended Data Fig. 3b)**. Necrosis, lymph node involvement, lymphovascular invasion, pathological tumor size, Ki67 labelling indices, non-adenocarcinoma histology and total cell-free DNA input predicted ctDNA detection in univariable analyses (**Extended Data Fig. 3c**). Multivariable analysis revealed non-adenocarcinoma histology, the presence of lympho-vascular invasion and high Ki67 proliferation index as independent predictors of ctDNA detection (**Extended Data Fig. 3c**). Since FDG-avidity on positron emission tomography (PET) scans correlates with proliferative indices in early-stage NSCLC[13,14], we investigated tumor PET FDG-avidity and ctDNA detection. PET FDG-avidity predicted ctDNA detection (area under curve = 0.84, $P<0.001$, n=92) (**Extended Data Fig. 3d**). Within LUADs, driver events in *KRAS*, *EGFR* or *TP53* were not associated with ctDNA detection (**Extended Data Fig. 3e).**

We analyzed the distribution of clonal and subclonal SNVs in ctDNA positive patients. Clonal SNVs were detected in all 46 ctDNA positive patients and a median of 94% (range 11% to

100%) of clonal SNVs targeted by assay-panels were detected in the ctDNA of these patients. 40 of 46 ctDNA positive patients had subclonal SNVs targeted by assay-panels and subclonal SNVs were detected in 27 (68%) of these patients. A median of 27% (range 0% to 91%) of subclonal SNVs within individual assay-panels were detected in ctDNA positive patients **(Fig. 2b)**. The mean plasma variant allele frequency (VAF) of clonal SNVs was higher than that of subclonal SNVs **(Extended Data Fig. 4a,** within patient comparison, Wilcoxon signed-rank test, P<0.001, n=27, **Supplementary Table 2**) supporting the use of clonal alterations as a more sensitive method of ctDNA detection than subclonal alterations[10,15].

In ctDNA positive patients, pathologic tumor size correlated with mean clonal plasma VAF (Spearman's Rho = 0.405, P=0.005, n=46, **Extended Data Fig. 4b**). CT scan volumetric analyses were available in 38 of 46 ctDNA positive patients (see **Extended Data Fig. 4c**). Tumor volume correlated with mean clonal plasma VAF (**Fig 3a,** Spearman's Rho = 0.61, P<0.001, n=38). A linear relationship between log- transformed volume and log- transformed mean clonal VAF values was observed (**Fig. 3a**). The line of best fit applied to the data was consistent with the line fitted to NSCLC volumetric data and ctDNA plasma VAFs reported in previously published work[16] (**Extended Data Fig. 4d**). Linear modelling based on the TRACERx data predicted that a primary tumor burden of $10cm^3$ would result in a mean clonal

236 plasma VAF of 0.1% (95% C.I. 0.05 to 0.17%) **(Fig. 3b).** Tumor purity was multiplied by
237 tumor volume to control for stromal contamination to determine cancer cell volume
238 corresponding to clonal plasma VAF (**Extended Data Fig. 4e**). On the assumption that $1cm^3$
239 of pure tumor contains 9.4×10^7 cells[17], a plasma VAF of 0.1% would correspond to a primary
240 NSCLC malignant burden of 326 million cells **(Fig 3b, Extended Data Fig. 4f).**

241 To investigate predictors of subclone detection, detected subclonal SNVs were mapped back
242 to M-seq derived tumor phylogenetic trees. 35 of 57 (61%) shared subclones (identified in more
243 than one tumor region through M-Seq analysis) were identified in ctDNA, compared with 26
244 of 80 (33%) private subclones (detected in a single tumor region only) **(Extended Data Fig**
245 **4g)**. This suggested subclone volume influences subclonal ctDNA detection. Subclone volume
246 was estimated based on mean regional subclone cancer cell fraction and cancer cell volume.
247 Detected subclonal SNVs mapped to subclones with higher estimated volumes than subclones
248 containing undetected SNVs (**Fig. 3c)** and subclone volume correlated with subclonal SNV
249 plasma VAF (**Fig. 3d**).

250 **Detecting and characterizing NSCLC relapse**

The longitudinal phase of the study aimed to determine if ctDNA profiling with patient-specific assay panels could detect and characterize the branched subclone(s) seeding NSCLC relapse. Pre- and post-surgical plasma ctDNA profiling was performed blinded to relapse status in a sub-group of 24 patients (cohort characteristics, **Extended Table 1d-e**). This included relapse free patients who had been followed-up for a median of 775 days (range 688 to 945 days, n=10) and confirmed NSCLC relapse cases (n=14) (cohort design, **Extended Data Fig. 2c**). Additional PCR assays were added to panels in this phase of the study to attempt to improve ctDNA detection in LUADs, a median of 18.5 SNVs (range 12 to 20) were targeted by LUSC assay-panels and a median of 28 SNVs (range 25 to 30) were targeted by LUAD assay-panels (**Extended Data Fig. 2d-e).**

Patients were followed up with three to six monthly clinical assessment and chest radiographs. At least 2 SNVs were detected in 13 of 14 (93%) patients with confirmed NSCLC relapse prior to, or at, clinical relapse **(Fig 4a-g, Extended Data Fig. 5)**. At least two SNVs were detected in 1 of 10 (10%) patients (CRUK0013) with no clinical evidence of NSCLC relapse (**Fig. 4h, Extended Data Fig. 6)**. Excluding a single case where no post-operative plasma was taken prior to clinical relapse (CRUK0041), the median interval between ctDNA detection and NSCLC relapse confirmed on clinically indicated CT imaging (lead-time) was 70 days (range

10 to 346 days). Four of 13 relapse cases exhibited lead-times of more than six months (**Fig. 4a-d**). In two cases ctDNA detection preceded CT imaging inconclusive for NSCLC relapse by 157 days (CRUK0004, **Fig 4b**) and 163 days (CRUK0045, **Fig 4d**). ctDNA profiling reflected adjuvant chemotherapy resistance - CRUK0080, CRUK0004 and CRUK0062 had detectable ctDNA in plasma within 30 days of surgery. The number of detectable SNVs increased in all three cases despite adjuvant chemotherapy, with disease recurring within 1 year of surgery **(Fig. 4a-c)**. In contrast, CRUK0013 had 20 SNVs detectable in ctDNA 72 hours after surgery and 13 SNVs detectable prior to adjuvant chemotherapy; 51 days following completion of adjuvant treatment and at post-operative days 457 and 667 no SNVs were detectable and the patient remains relapse free 688 days post-surgery **(Fig. 4h).** ctDNA profiling detected intracerebral relapse; CRUK0029 had a PET scan performed 50 days prior to surgery demonstrating normal cerebral appearances. ctDNA remained detectable following surgery, 54 days post-operatively the patient was diagnosed with intracerebral metastasis, no extracranial disease was evident on CT imaging **(Fig. 4e).**

We sought to resolve subclonal evolutionary-dynamics associated with NSCLC relapse. Subclonal SNVs displaying plasma VAFs similar to clonal SNVs from clusters confined to a single phylogenetic branch, were detected post-operatively in the ctDNA of four patients who

suffered NSCLC relapse (CRUK0004, CRUK0063, CRUK0065 and CRUK0044) **(Fig. 4b,f-g, Extended Data Fig 5b).** This suggested a relapse process dominated by one subclone represented in our assay-panel. The subclone implicated by ctDNA as driving the relapse in the case of CRUK0004 contained an ERRB2 (HER2) amplification event (>15 copies, triploid background), that may be targetable in NSCLC[18] **(Fig. 4b).** Relapses involving subclones from more than one phylogenetic branch were evident in patients CRUK0080, CRUK0062 **(Fig. 4a,c)** and CRUK0041 (**Extended Data Fig 5c**)**.**

Validation of phylogenetic characterization

To validate subclonal ctDNA analyses, data acquired from sequencing metastatic tissue at recurrence was integrated with M-seq primary tumor data (for biopsy details, **Supplementary Table 3**). Patient CRUK0063 suffered para-vertebral relapse of their NSCLC. Post-operative ctDNA analysis revealed the detection of the same subclonal SNV (*OR5D18*) on four consecutive occasions over a 231-day period **(Extended Data Fig. 7a)**. The *OR5D18* SNV traced back to a subclonal cluster private to primary tumor region three (**Fig. 5a**). CT-guided biopsy tissue was acquired from the para-vertebral metastasis at post-operative day 467. Exome sequencing of relapse tissue revealed the subclonal cluster containing the *OR5D18* SNV gave rise to the metastatic subclone (**Fig. 5a**), this supported ctDNA phylogenetic characterization

of relapse. The para-vertebral biopsy contained 88 SNVs not called as present in the primary tumor including an *ARID1A* stop-gain driver SNV. Re-examination of primary tumor region M-Seq data with a lower SNV calling threshold revealed that 16 of 88 SNVs, including *ARID1A,* were detectable in primary tumor region three, compared to a maximum of 2 of 88 in other tumor regions **(Extended Data Fig. 7b).** These data suggest that ctDNA profiling can resolve the primary tumor region from which a low frequency metastatic subclone derives. CRUK0035 developed two liver and one adrenal metastases **(Fig. 5b)**. Sequencing of the metastatic liver deposit revealed that only 109 of 149 SNVs classed as clonal in the primary tumor were detectable in the metastasis. This was suggestive of an ancestral branching event not resolved through primary M-seq analysis **(Fig 5b)**. Post-operative ctDNA profiling identified clonal SNVs present in the liver metastasis biopsy but also revealed SNVs representing a subclone from the primary tumor (**Extended Data Fig 7c)**. This subclone was not present in the metastatic liver deposit **(Fig 5b)**. These data may reflect ctDNA identified from the non-biopsied metastases suggesting multiple metastatic events. CRUK0044 suffered a vertebral and right hilar relapse. Post-operatively the same subclonal SNV (*OR10K1*), was detected in ctDNA on two occasions 85 days apart **(Extended Data Fig. 7d)**. This SNV was represented in a single subclone detected through sequencing hilar lymph-node metastatic

319 tissue, supporting ctDNA findings (**Fig. 5c**). CRUK0041 suffered an intracerebral, hilar and
320 subcarinal lymph node relapse. Four subclonal SNVs representing both branches of the tumor
321 phylogenetic tree were detectable in ctDNA at relapse. Consistent with these data, sequencing
322 of subcarinal metastatic tissue revealed the presence of subclonal SNVs mapping to both
323 phylogenetic branches **(Fig 5d, Extended Data Fig. 7e).** Patient CRUK0013 had detectable
324 ctDNA 3 and 38 days post-operatively. Following adjuvant chemoradiotherapy for lymph-node
325 metastases identified in the pathological specimen, ctDNA levels became undetectable (**Fig**
326 **4h**). Two involved lymph-nodes were sampled for exome analysis together with M-seq of the
327 primary tumor. Four subclonal SNVs detected in ctDNA post-operatively mapped to an
328 ancestral subclone (describing a subclone that existed during the tumor's evolution) (**Extended**
329 **Data Fig. 7f)**. This ancestral subclone contained a KRAS amplification (>15 copies, triploid
330 background) and was identified as present in primary tumor and sampled lymph-nodes by M-
331 Seq **(Fig. 5e).** These data provide phylogenetic characterization of post-operative residual
332 disease that responded to adjuvant chemoradiotherapy (**Fig. 4h**).

333 **ctDNA profiling in the metastatic setting**

Patient CRUK0063 underwent examination through the PEACE post-mortem study 24 hours following death. M-Seq data from the six post-mortem tumor regions (para-aortic, para-vertebral and lung metastases, day 857), the para-vertebral relapse biopsy (day 467) and five primary tumor regions (day 0) were combined to infer the phylogenetic structure of this patient's NSCLC (**Fig. 6a**). All seven metastatic tumor regions arose from a single ancestral subclone represented by phylogenetic cluster 8. Six metastatic regions shared a later phylogenetic origin, cluster 12 (**Fig. 6b)**. The single tumor region not containing phylogenetic cluster 12 was sampled from the para-aortic metastasis at autopsy and contained a private subclone represented by phylogenetic cluster 9 (**Fig. 6b).**

We designed a bespoke ctDNA assay-panel to retrospectively track metastatic subclonal burden. 20 clonal SNVs and a median of 8 subclonal SNVs (range 4 to 15) in each of 9 metastatic subclonal clusters were targeted by the assay-panel **(Extended Data Fig. 8).** Since 103 variants per time-point were profiled, SNV detection thresholds were increased to maintain platform specificity (**see Methods**). This resulted in a predicted false positive rate (FPR) of 0.0011 translating to a 10.7% risk of a single false-positive SNV at each time point and a 0.5% risk of 2 false-positive SNVs at each time point when testing 103 SNVs.

Two clonal SNVs were detected by the 103 SNV assay-panel at day 151 post-surgery **(Fig 6c, Extended Data Fig. 8)**, 189 days prior to the time point ctDNA was detected using the 19 SNV assay-panel in **Figure 4f**. At day 242 a single subclonal SNV was detected from phylogenetic cluster 8 **(Fig 6c, Extended Data Fig. 8)**, within the context of a 10.7% false-positive risk a single SNV call could represent type I error. At day 466, following clinical-relapse at the thoracic para-vertebral site, 18 of 20 SNVs mapping to phylogenetic clusters (8,11 and 12) were detected in ctDNA, these subclonal clusters were shared between six of seven metastatic sites **(Fig 6b-c**, **Extended Data Fig. 8**). Single SNVs from two private subclones (phylogenetic cluster 5 and 9) were also detectable in ctDNA at day 466 **(Fig 6c, Extended Data Fig. 8)**. These subclones were not identified in the CT guided para-vertebral biopsy taken at day 467 (**Fig. 6b)**. The mean plasma VAF of the SNVs detected in phylogenetic clusters 11, 8, 12, 9 and 5 mirrored their proximity to the clonal cluster (light blue) in the M-Seq derived phylogenetic tree **(Fig. 6a,c)**. This suggested a tiered burden of subclonal disease concordant with M-seq phylogenetic inferences**.** Mean clonal VAF fell in response to palliative radiotherapy and chemotherapy, but at day 767 increased **(Fig. 6c)**. Single SNVs mapping to phylogenetic clusters 5 and 9 and two SNVs mapping to phylogenetic cluster 2 were now detectable in ctDNA 90 days before death **(Fig. 6a-c, Extended Data Fig 8).** These three

phylogenetic clusters represented subclones private to the para-aortic metastases **(Fig 6. a-b)**. Consistent with these data significant para-aortic progression was observed at post-mortem compared with most recent CT imaging performed 112 days before death - which showed no evidence of para-aortic disease.

Discussion

In summary, we find predictors of ctDNA detection in early-stage NSCLC characterized by non-adenocarcinoma histology, necrosis, increased proliferative indices and lymphovascular invasion. Triple negative breast cancers display necrosis[19], high proliferative indices[20,21] and are associated with increased ctDNA levels compared with other breast cancer subtypes[6] suggesting extension of these observations beyond NSCLC.

Tumor volume correlated with plasma ctDNA VAF (**Fig 3a.**). A primary NSCLC tumor volume of $10cm^3$ predicted a ctDNA plasma VAF of 0.1%; the VAF conferring optimum sensitivity for most ctDNA platforms. Low-dose CT lung screening can identify lung nodules with diameters from 4mm[22]. Assuming a spherical nodule this would translate to a tumor volume of $0.034cm^3$. Based on the relationship between tumor volume and ctDNA plasma VAF observed in this study a tumor volume of 0.034cm3 would equate to a plasma VAF of

383 1.4 x 10^{-4} % (95% CI, 6.4 x 10^{-6} to 0.0031%), at the extreme of detection limits of current
384 ctDNA platforms[23]. Sensitivity of clonal SNV ctDNA directed early NSCLC screening may
385 therefore be constrained by tumor size using current technologies.

386 A limitation to targeted ctDNA profiling is cost, estimated at $1750 per patient for sequencing
387 a single tumor region, synthesis of a patient-specific assay-panel and profiling of five plasma
388 samples. Adjuvant platinum-based chemotherapy in NSCLC improves cure rates following
389 surgery in only 5% of patients and 20% patients receiving chemotherapy experience acute
390 toxicities[3]. There is a need to increase adjuvant therapy efficacy and better target its use.
391 Bespoke ctDNA profiling can characterize the subclonal dynamics of relapsing NSCLC and
392 identify adjuvant chemotherapy resistance. These findings indicate that drug development
393 guided by ctDNA platforms to identify residual disease, define adjuvant treatment response
394 and target emerging subclones prior to clinical recurrence in NSCLC, with appropriate CLIA
395 validation, are now feasible.

396

397 **Supplementary information** is available in the online version of the paper

Acknowledgements We dedicate this manuscript to the memory of Roberto Macina. We thank Samantha Navarro and Antony Tin for facilitating the PEACE ctDNA analysis. We thank the members of the TRACERx and PEACE consortia (see Supplementary 4 for list of investigators) for participating in this study. C.S. is Royal Society Napier Research Professor. This work was supported by the Francis Crick Institute which receives its core funding from Cancer Research UK (FC001169), the UK Medical Research Council (FC001169) and the Wellcome Trust (FC001169); by the UK Medical Research Council (grant reference MR/FC001169 /1); CS is funded by Cancer Research UK (TRACERx and CRUK Cancer Immunotherapy Catalyst Network), the CRUK Lung Cancer Centre of Excellence, Stand Up 2 Cancer (SU2C), the Rosetrees Trust, NovoNordisk Foundation (ID 16584), the Prostate Cancer Foundation, the Breast Cancer Research Foundation, the European Research Council (THESEUS) and Support was provided to CS by the National Institute for Health Research, the University College London Hospitals Biomedical Research Centre and the Cancer Research UK University College London Experimental Cancer Medicine Centre.

Authorship contribution statement

C.A., N.J.B., G.A.W., M.J-H., T.C., R.S., and J.L-Q. contributed equally to this work. C.A. and C.S. co-wrote the manuscript. C.A., M.J.H., and C.S. conceived study design. C.A., N.J.B.,

G.A.W. and R.R. integrated clinicopathological data, exome data and ctDNA data. B.G.Z, J.L., T.C., R.S., E.K., N.S., D.H., A.N. and A.P., conducted and analysed multiplex-PCR NGS experimental work. N.J.B, G.A.W, T.B.K.W, R.R., and N.M. conducted M-Seq analyses of exome data. J.L-Q, T.M. and D.A.M. conducted pathological review. F.F., R.E. and F.Z. conducted radiological review of PET scans. H.J.W.L.A., W.L.B., F.M.F. and N.J.B. conducted radiomic analyses. S.V., D.J., J.L., S.S., J.C-K., A.R., T.C., D.O. and A.A. conducted TRACERx sample processing. G.E., S.W., N.M. and G.A.W. conducted exome sequencing. L.M., J.R. and J.S. conducted ctDNA cross-platform validation. M.J.H., C.D., J.S. and C.S. designed study protocols. C.H., S.L.M., M.F., T.A., M.Fa., E.B., D.L., M.H., S.K., N.P., S.M.J., R.T., A.A., F.B., Y.S., R.S., L.J., A.M.Q, P.C., B.N., G.M., G.L., S.T., M.N., H.R., K.K., M.C., L.G., D.F., A.N., S.R., G.A., S.K., P.R., V.E., B.I., M.I-S., V.P., J.L., M.K., R.A., H.A., H.D., S.L. are clinical members of TRACERx study sites. J.H. and H.L. run the UCL GCLP facility. A.H., H.B., N.I. and Y.N. were involved in study oversight. J.A.S., J.L-Q., Z.S., E.G., S.K., S.T., M.A.B, R.F.S., J.H., A.S., S.Q., P.V.L., C.D. and J.L. gave advice and reviewed the manuscript. A.H. gave statistical advice. C.S. provided overall study oversight.

Author information

The authors declare competing financial interests. Reprints and permissions information is available at www.nature.com/reprints. Correspondence should be addressed to C.S. (Charles.Swanton@crick.ac.uk).

References

1. Jemal A, Bray F, Center MM, Ferlay J, Ward E, Forman D. Global cancer statistics. CA: A Cancer Journal for Clinicians 2011;61(2):69-90.

2. Siegel RL, Miller KD, Jemal A. Cancer statistics, 2017. CA: A Cancer Journal for Clinicians 2017;67(1):7-30.

3. Pignon J-P, Tribodet H, Scagliotti GV, Douillard J-Y, Shepherd FA, Stephens RJ, et al. Lung Adjuvant Cisplatin Evaluation: A Pooled Analysis by the LACE Collaborative Group. Journal of Clinical Oncology 2008;26(21):3552-9.

4. Landau Dan A, Carter Scott L, Stojanov P, McKenna A, Stevenson K, Lawrence Michael S, et al. Evolution and Impact of Subclonal Mutations in Chronic Lymphocytic Leukemia. Cell;152(4):714-26.

446 5. Beaver JA, Jelovac D, Balukrishna S, Cochran RL, Croessmann S, Zabransky DJ, et
447 al. Detection of Cancer DNA in Plasma of Patients with Early-Stage Breast Cancer. Clinical
448 Cancer Research 2014;20(10):2643-50.

449 6. Garcia-Murillas I, Schiavon G, Weigelt B, Ng C, Hrebien S, Cutts RJ, et al. Mutation
450 tracking in circulating tumor DNA predicts relapse in early breast cancer. Science
451 Translational Medicine 2015;7(302):302ra133-302ra133.

452 7. Tie J, Wang Y, Tomasetti C, Li L, Springer S, Kinde I, et al. Circulating tumor DNA
453 analysis detects minimal residual disease and predicts recurrence in patients with stage II
454 colon cancer. Science Translational Medicine 2016;8(346):346ra92-ra92.

455 8. Jamal-Hanjani M, Hackshaw A, Ngai Y, Shaw J, Dive C, Quezada S, et al. Tracking
456 genomic cancer evolution for precision medicine: the lung TRACERx study. PLoS Biol
457 2014;12(7):e1001906.

458 9. Jamal-Hanjani M. TRACERx – Tracking Non-Small Cell Lung Cancer Evolution.
459 New England Journal of Medicine (accepted, in press) 2017.

460 10. Jamal-Hanjani M, Wilson GA, Horswell S, Mitter R, Sakarya O, Constantin T, et al.
461 Detection of ubiquitous and heterogeneous mutations in cell-free DNA from patients with
462 early-stage non-small-cell lung cancer. Annals of Oncology 2016;27(5):862-7.

463 11. Jr LAD, Bardelli A. Liquid Biopsies: Genotyping Circulating Tumor DNA. Journal of
464 Clinical Oncology 2014;32(6):579-86.

465 12. Caruso R, Parisi A, Bonanno A, Paparo D, Quattrocchi E, Branca G, et al. Histologic
466 coagulative tumour necrosis as a prognostic indicator of aggressiveness in renal, lung, thyroid
467 and colorectal carcinomas: A brief review. Oncology Letters 2012;3(1):16-8.

468 13. Vesselle H, Schmidt RA, Pugsley JM, Li M, Kohlmyer SG, Vallières E, et al. Lung
469 Cancer Proliferation Correlates with [F-18]Fluorodeoxyglucose Uptake by Positron Emission
470 Tomography. Clinical Cancer Research 2000;6(10):3837-44.

471 14. Higashi K, Ueda Y, Yagishita M, Arisaka Y. FDG PET measurement of the
472 proliferative potential of non-small cell lung cancer. The Journal of Nuclear Medicine
473 2000;41(1):85.

15. Murtaza M, Dawson S-J, Pogrebniak K, Rueda OM, Provenzano E, Grant J, et al. Multifocal clonal evolution characterized using circulating tumour DNA in a case of metastatic breast cancer. Nature Communications 2015;6:8760.

16. Newman AM, Bratman SV, To J, Wynne JF, Eclov NCW, Modlin LA, et al. An ultrasensitive method for quantitating circulating tumor DNA with broad patient coverage. Nat Med 2014;20(5):548-54.

17. Del Monte U. Does the cell number 109 still really fit one gram of tumor tissue? Cell Cycle 2009;8(3):505-6.

18. Peters S, Zimmermann S. Targeted therapy in NSCLC driven by HER2 insertions. Translational Lung Cancer Research 2014;3(2):84-8.

19. Livasy CA, Karaca G, Nanda R, Tretiakova MS, Olopade OI, Moore DT, et al. Phenotypic evaluation of the basal-like subtype of invasive breast carcinoma. Mod Pathol 2005;19(2):264-71.

20. Keam B, Im S-A, Kim H-J, Oh D-Y, Kim JH, Lee S-H, et al. Prognostic impact of clinicopathologic parameters in stage II/III breast cancer treated with neoadjuvant docetaxel

and doxorubicin chemotherapy: paradoxical features of the triple negative breast cancer. BMC Cancer 2007;7:203-.

21. Rhee J, Han SW, Oh DY, Kim JH, Im SA, Han W, et al. The clinicopathologic characteristics and prognostic significance of triple-negativity in node-negative breast cancer. BMC Cancer 2008;8:307.

22. Team TNLSTR. Reduced Lung-Cancer Mortality with Low-Dose Computed Tomographic Screening. New England Journal of Medicine 2011;365(5):395-409.

23. Newman AM, Lovejoy AF, Klass DM, Kurtz DM, Chabon JJ, Scherer F, et al. Integrated digital error suppression for improved detection of circulating tumor DNA. Nat Biotech 2016;34(5):547-55.

Figure 1. Phylogenetic ctDNA tracking

Overview of the study methodology. Multi-region sequencing of NSCLC was performed as part of the TRACERx study. PCR assay-panels were designed based on phylogenetic analysis, targeting clonal and subclonal single nucleotide variants to facilitate non-invasive tracking of the patient-specific tumor phylogeny. Assay-panels were combined into multiplex assay-pools containing primers from up to 10 patients. Cell-free DNA was extracted from pre- and post-

operative plasma samples and multiplex-PCR performed, followed by sequencing of amplicons. Findings were integrated with M-Seq exome data to track tumor evolution.

Figure 2. Clinicopathological predictors of ctDNA detection

a) Heatmap showing clinicopathological and ctDNA detection data, continuous variables quartiled. Raw data and patient IDs in attached worksheet. b) Detection of clonal and subclonal single nucleotide variants within 46 patients with two or more single nucleotide variants detected in plasma. Histology indicated in panels as LUSC, LUAD and Other.

Figure 3. Tumor volume predicts plasma variant allele frequency

a) Tumor volume (cm^3) measured by CT volumetric analysis correlates with mean clonal plasma VAF, n=38, grey vertical lines represent range of clonal VAF, red shading indicates 95% confidence intervals. b) Predicted mean clonal VAF at hypothetical volumes ranging from 1 to 100cm^3 based on model in panel a, predicted cancer cell number based on model in extended data 4e. c) Estimated effective subclone size, defined as mean CCF of subclone multiplied by tumor volume and purity, influences subclonal SNV detection. For negative calls, median effective subclone size was 1.70 cm^3, range= 0.21-24.11, n=163, for positive calls, median effective subclone size = 4.06 cm^3, range = 0.31 – 49.20, n=109. Wilcoxon rank sum

test, P<0.001, data from 34 patients (passed volumetric filters with subclonal SNVs represented in assay-panel). d) Estimated effective subclone size correlates with subclonal plasma VAF, n=109 subclonal SNVs, data from 34 patients (passed volumetric filters with detected subclonal SNVs in plasma).

Figure 4. Post-operative ctDNA detection predicts and characterizes NSCLC relapse

a-h) Longitudinal cell-free DNA profiling. Circulating tumor DNA (ctDNA) detection in plasma was defined as the detection of two tumor-specific SNVs. Detected clonal (circles, light blue) and subclonal (triangles, colors indicates different subclones) SNVs from each patient-specific assay-panel are plotted on graphs colored by M-Seq derived tumor phylogenetic nodes. Mean clonal (blue) and mean subclonal (red) plasma VAF are indicated on graphs as connected lines. Pre-operative and relapse M-Seq derived phylogenetic trees represented by ctDNA are illustrated above each graph.

Figure 5. **Phylogenetic trees incorporating relapse tissue sequencing data**

Phylogenetic trees based on mutations found in primary and metastatic tissue (a-d), or primary tumor and lymph node biopsies (e). Colored nodes in phylogenetic trees indicate cancer clones harboring mutations assayed for in ctDNA, grey indicates a clone not assayed.

Branch length is proportional to number of mutations unless crossed. Dashed red lines show branches leading to metastatic relapse. Colored bars below show the number of assays per sample detected preoperatively and at relapse (a-d) or in the absence of relapse, post-surgery (e). Thin colored bar shows number of assays in total. Colors match clones on the phylogenetic trees.

Figure 6. ctDNA tracking of lethal cancer subclones in CRUK0063

Phylogenetic analysis of one relapse biopsy (day 467) and five metastatic biopsies (post mortem) **a)** To-scale phylogenetic tree of CRUK0063 including M-seq based on metastatic and primary tumor regions. Branch length is proportional to number of mutations in each subclone. **b)** Phylogenetic trees matching metastatic lesions, colored nodes represent mutation clusters found at each site and assayed for in ctDNA. Open circles represent mutation clusters not detected in ctDNA. **c)** Tracking plot showing mean VAF of identified mutation clusters in ctDNA. Size of dots indicates number of assays detected. Colors correspond to mutation clusters and match panels **a**) and **b**).

Methods

Patients and samples

The cohort of 100 patients evaluated within this study comprises the first 100 patients prospectively analyzed by the lung TRACERx study (Clinicaltrials.gov no: NCT01888601, approved by an independent Research Ethics Committee, 13/LO/1546) and mirrors the prospective 100 patient cohort by Jamal-Hanjani M et al[9]. All surgically resected primary tumor samples were macroscopically reviewed by a pathologist. Spatially separated tumor regions, documented by photography, were collected and snap frozen in liquid nitrogen for subsequent DNA extraction. Relapse tissue samples, excess to diagnostic requirements, were acquired via clinical procedures including CT guided biopsy and endoscopic bronchial ultrasound guided biopsy. Fresh tissue for research was snap frozen immediately following acquisition for subsequent DNA extraction. Post mortem examination was performed through the PEACE study within 24 hours of death (Clinicaltrials.gov no: NCT03004755, approved by an independent Research Ethics Committee, 13/LO/0972). Details on relapse tissue sampling available in Supplementary Table 3. Informed consent was obtained from all subjects in this study.

Tissue microarray creation and Ki67 immunohistochemistry

Tissue microarrays (TMAs) were created of 100 NSCLC cases for $Ki67^+$ immunohistochemistry. Representative tumor areas were defined by examination of H&E stained sections from all 100 tissues blocks. From each NSCLC case two 2mm cores were selected from different regions within each specimen and re-embedded in recipient blocks, resulting in a TMA of 200 cores with four normal lung cores as negative control. 2-5µm sections from tissue-microarrays containing tumor were cut. Immunohistochemistry with anti-Ki67 monoclonal antibody (Dilution 1:100; clone MIB-1; DAKO Agilent Technologies LDA, UK Limited, Stockport, Cheshire SK8 3GR, UK) was performed using BenchMark Ultra (Ventana/Roche). The percentage of Ki67 positive cells were averaged across two tumor sections for each case. Detection was performed using the peroxidase-based detection reagent conjugate (OptiView DAB IHC Detection Kit; Ventana Medical Systems, Inc).

Central histopathological review

Digital images of tumor sections from all cases were reviewed in detail centrally by at least one pathologist, and in cases of uncertainty, by two. Percentage of necrosis and the presence of lymphovascular invasion were all evaluated on digital images from scanned diagnostic slides blinded to the ctDNA detection status of the patient in question.

Central radiology review & volume estimation

92 of 96 anonymized diagnostic PET-CT were retrospectively reviewed by a Nuclear Medicine Physician, blinded to the initial PET-CT reports. Scan images were not available in three cases (CRUK0025, CRUK0039 and CRUK0023) and in one case a pre-operative PET-CT was not performed (CRUK0082). CT and PET images were matched and fused into transaxial, coronal and sagittal images and reviewed on a dedicated PET/CT software visualizer (AW 4.1/4.2 GE medical systems). The semi-quantitative parameter Standardized Uptake Value (SUV) max for the primary tumor mass was calculated and recorded along with SUV_{max} of mediastinal background uptake. Tumor-to-background ratio (TBR) was calculated based on SUV_{max} of the tumor divided by mediastinal background uptake[24,25]. Tumor volume was determined based on tumor CT scans. CT slices of the primary tumor were measured with 3D Slicer applying the "lung algorithm window" settings, tumor contours were segmented on each axial CT slice. These steps were performed by an experienced resident (W.L.B.), and all contours were confirmed and edited where necessary, by a radiologist with 14 years of experience in cancer imaging (F.M.F.). Effective tumor volume was defined as tumor volume multiplied with the mean purity of the tumor based on M-seq, purity estimates derived from ASCAT analysis as

described[9]. Effective subclone size was defined as mean cancer cell fraction (CCF) across the regions of the mutation cluster multiplied by tumor volume and mean tumor purity.

DNA extraction & quantification

For cell-free DNA (cfDNA) extraction, blood samples were collected in K2 EDTA tubes. Samples were processed within 2 hours of collection by double spinning of blood first at 10 minutes at 1000g then plasma 10 minutes at 2000g. Plasma was stored in 1ml aliquots at –80ºC. Up to 5ml of plasma per case was available for this study (range 1-5ml, median 5 ml). The entire volume of plasma was used for cfDNA extraction. cfDNA was extracted using the QIAamp Circulating Nucleic Acid kit (Qiagen) and eluted into 50 µl DNA Suspension Buffer (Sigma). The purified cfDNA was stored at -20ºC until use. Genomic DNA was extracted from each tumor region as described[9]. Every cfDNA sample was QCed and quantified on the Bioanalyzer High Sensitivity (Agilent) using a standard curve generated from pre-quantified mono-nucleosomal DNA samples. Plasma cfDNA consists of a main mono-nucleosomal peak (~160 bp); for some samples, di-nucleosomal and tri-nucleosomal peaks are visible (at ~320 bp and ~500 bp, respectively). The library prep method used selectively amplifies the mono-nucleosomal fraction of cfDNA.

Exome sequencing and processing

Whole exome sequencing was performed on DNA purified from tumor tissue and normal blood as described[9], with the exception of CRUK0063_BR_T1-R1. This capture was performed according to the manufacturer's 200 ng DNA protocol (Agilent). Annotated SNV calls are available in Supplementary Table 3 in Jamal-Hanjani et al. 2017[9]. For this study, one relapse sample was acquired through metastatic tissue biopsies from each of four patients (CRUK0035, CRUK0041, CRUK0044, CRUK0063). Additionally, six metastatic samples were acquired at post mortem examination of CRUK0063. Genomic DNA was purified from all tissue samples, and processed through the TRACERx bioinformatics pipeline as described[9]. Annotated SNV calls are available in Supplementary Table 5.

SNV assay design

The Natera assay design pipeline was used to generate forward and reverse PCR primers for all somatic SNVs detected in tumor samples. The assays were combined into pools such that any primer pair in a pool is not predicted to form primer dimers. In this way 10 balanced pools were created, each containing the assays for 10 patients' SNVs. For each patient, assays were prioritized such that, 1) assays covering driver SNVs had highest priority, and 2) there was uniform sampling of phylogenetic tree. For the longitudinal cohort, up to 10 extra assays were

633 generated for adenocarcinoma samples. SNV assays were ordered from IDT (Coralville, IA)
634 as individual oligos in 96-well plates, desalted and normalized to 100 μM each. The oligos
635 were pooled according to the pooling strategy previously described[10] and each pool was QC-
636 ed by running the multiplex PCR and sequencing protocol using one plasma cfDNA library
637 from a healthy subject. For each pool, the sequencing data was analyzed to determine the
638 amount of primer-dimer reads and to identify drop-out assays. Primers contributing to dimer
639 formation were removed from each final pool.

640 **Analytical validation**

641 Synthetic spikes representing twenty SNVs randomly selected from Pool 1 were designed and
642 synthesized (IDT, Coralville, IA) as 160 bp oligos with the respective SNV placed in the middle
643 (position 80). These synthetic spikes were mixed at equimolar ratios and used to prepare a
644 library. This library was titrated into a library prepared from mono-nucleosomal DNA (10,000
645 copies) from a normal cell line (AG16778 from Coriell, Camden, NJ). The library of 20
646 synthetic spikes was titrated into the mononucleosomal DNA library at 2.5%, 0.5%, 0.25%,
647 0.1%, 0.05% and 0% (each in triplicate), and 0.01%, 0.005% and 0.001% (each in
648 quadruplicate. Because preparing spiked samples at such low levels is either subject to
649 sampling noise (0.01% spikes into 10,000 genomic copies background is equivalent to one

mutant copy), or is not possible (at levels less than 0.01%), samples were mixed as libraries. Following library mixing and sequencing, data was analyzed to detect all the targets in Pool 1 using the same parameters as used for the patient samples. Targets that had a depth of read less than the threshold were not analyzed. The measured VAF of each spike for the samples with 2.5% nominal input was used to calculate an input correction factor (measured VAF/2.5%); that was applied to the other inputs of the corresponding spike titration series. The measured VAF differed from the nominal input most likely because the mononucleosomal fragmentation pattern is not entirely random. Because of this, the actual input levels differ from the nominal input levels, and the sensitivity is measured based on corrected input intervals (chosen such that there are a meaningful number of samples in each interval). Sensitivity of >99% at SNV input frequencies down to 0.1% was achieved (199 SNVs detected out of 201 eligible positive positions), with a specificity of 99.6% for all negative SNV positions (19 false positive SNVs called out of 5099 eligible positions).

Plasma SNV mPCR-NGS workflow

Forty microliters of the extracted cfDNA from each case was used as input into library preparation using the Natera Library Prep Kit. All purified libraries were QC-ed on the LabChip GX 5k DNA chip. Successful libraries had a single peak at ~250 bp. The amplified

libraries were then analyzed by mPCR-NGS. Optimal mPCR conditions were as described. Each PCR assay pool was used to amplify the SNV targets from the 10 corresponding samples and 20 negative control samples (plasma libraries prepared from healthy subjects). Each amplicon pool was sequenced on one Illumina HiSeq 2500 Rapid Run with 50 cycles paired-end reads using the Illumina Paired End v1 kit with an average target DOR of ~40,000 per assay.

Plasma SNV calling algorithm

The set of SNVs covered by the assays in a pool were considered as target SNVs for the corresponding sequencing run. Target assays with <1000 reads in the plasma samples were considered failed and were not analyzed further. At each SNV position, an error model was built using all of the 20 negative control samples plus the cancer samples that were not expected to contain that particular SNV (based on tumor-tissue sequencing). Samples with high plasma VAF (>20%) among the putative negatives were considered to have possible germline mutation and were excluded from the error model. A confidence score was calculated for each target SNV based on the error model. A positive plasma SNV call was made if the confidence score for that mutation in the corresponding plasma sample passed our confidence threshold. The SNVs called positive in plasma samples that were not expected to contain the given SNVs were

684 considered ‘false positive’, the false positive rate under these conditions was 0.24%. Notably,
685 there was no difference in depth of read between called and not called SNVs (Extended Data
686 Fig 1c). New assays were designed for CRUK0063 based on M-seq of metastatic biopsy
687 retrieved at day 467 and of metastatic lesions harvested post mortem. A total of 103 assays
688 were designed compared to 19 based on the primary tumor alone. An updated error threshold
689 was designed to control for false positives by using the original threshold to make SNV calls
690 on the negative samples in the run; the rate of calls were measured and defined as false-
691 positives. This false positive rate was then applied to the number of eligible positions in the
692 positive samples. This was repeated with more stringent thresholds until the expected number
693 of false positives in the eligible positions becomes ~1. All multiplex PCR-NGS ctDNA SNV
694 assays are available in Supplementary Table 6 (Baseline, pre-operative cohort assays),
695 Supplementary Table 7 (Longitudinal Assays), and Supplementary Table 8 (Extended
696 Longitudinal Assays for CRUK0063).

697 **Cross-platform validation using generic PCR-NGS panel section**

698 Cross-platform validation was performed in 28 patients with M-Seq confirmed SNV(s) within
699 one or more hotspots targeted by a generic multiplex PCR-NGS panel (Extended Table 2a-b,
700 Supplementary Table 9). 20ng of isolated cfDNA was used for library preparation using the

Oncomine™ Lung cfDNA Assay (ThermoFisher Scientific), according to the manufacturer's instructions. Automated template preparation and chip loading was conducted on the Ion Chef™ instrument using the Ion 520™ & Ion 530™ Kit-Chef (ThermoFisher Scientific). Ultimately, samples were sequenced on Ion 530™ chips using the Ion S5™ System (ThermoFisher Scientific). Sequencing data was accessed on the Torrent suite v5.2.2. Reads were aligned against the human genome (hg19) using Alignment v4.0-r77189, and variants were called using the coverage Analysis v4.0-r77897 plugin. All 18 bespoke-panel ctDNA negative patients had no tumor SNVs detectable in plasma pre-operatively by the generic panel supporting biological specificity of the bespoke targeted approach, 7 of 10 bespoke-panel ctDNA positive patients had tumor SNVs detected in plasma by the generic panel (Extended Table 2a-b). SNVs detected by hotspot panel not identified by M-Seq are displayed in Extended Table 2c.

Processing and phylogenetic analysis of relapse and primary tumor multiregion whole exome data

Biopsies from multiple regions from the primary tumor (n=327), metastatic biopsies (n=4) and matching blood germline samples (n=100) were subjected to multi-region whole exome sequencing and analysis including estimation of copy number, purity and ploidy, and

718 phylogenetic tree construction as described[9]. Briefly, phylogenetic analysis was performed
719 based on CCF determined for SNVs and clustered across tumor regions using a modified
720 version of Pyclone[9] into clusters with similar CCF values, filtered and processed as described[9].
721 Mutation clusters are assumed to represent tumor subclones, either current or ancestral, and are
722 used as input for construction of phylogenetic relationship. Phylogenetic trees were primarily
723 constructed using the published tool CITUP (0.1.0)[26]. However, in a small number of cases,
724 including all relapse/autopsy cases, manual tree construction was required and performed as
725 described[9]. Complete detail of primary tumor tree construction can be found in Jamal-Hanjani
726 et al. 2017[9]. Relapse tree construction was performed as follow: CRUK0063: clustering was
727 performed twice, once across 5 primary tumor regions and once across 5 primary, 1 relapse,
728 and 6 autopsy regions. To ensure consistency, when deriving a phylogenetic tree based on all
729 tumor regions, CCF clusters based on clustering only the primary tumor regions were
730 maintained for mutations not involved in metastatic relapse. A phylogenetic tree was
731 constructed based on 17 mutation clusters. CRUK0035: Clustering primary tumor regions with
732 the relapse region revealed one cluster private to the relapse, and one cluster shared with the
733 relapse and all other regions. CRUK0044: Clustering primary tumor regions with the relapse
734 region revealed a cluster private to the relapse, descended from a cluster private to region 1 in

the primary tumor. CRUK0041: Clustering primary tumor regions with the relapse region revealed cluster 4 as private to the relapse. This cluster must have evolved from cluster 3 only found in the relapse and in region 4. A private cluster 6 in region 4 must have evolved from cluster 4. However, this conflicts with clusters 2 and 5, found in the relapse and regions 1-3, but not region 4. This can be reconciled by assuming a polyclonal relapse, seeded primarily from regions 1-3, but with some contribution from cluster 3, private to region 4. Cluster data is available in Supplementary Table 5 under "PyClonePhyloCluster".

Statistical data analysis

Analysis was performed in the R statistical environment version 3.2.3 and SPSS version 24. All statistical tests were two-sided unless expressly stated. Multivariate logistic regression used detection of ctDNA (the dependent variable) classified as detection of 2 or more patient-specific variants in ctDNA and the covariates listed in Supplementary Table 1. All predictors were entered simultaneously into the regression. All continuous independent variables were found to be linearly related to the logit of the dependent variable (assessed via the Box-Tidwell procedure). The logistic regression model was statistically significant, $X^2(10) = 81.35$, $P<0.001$ and the Hosmer-Lemeshow P value was 0.9858 indicating that the model was not a poor fit. To determine the ability of PET TBR to predict whether or not tumor ctDNA was identified in

752 plasma, PET TBR estimates were analyzed by ROC curve analysis against binary detection of
753 ctDNA in plasma at baseline based on at least two variants detected, significance test based on
754 Wilcoxon rank sum test. For analysis involving longitudinally detected variants (Figure 4,
755 Extended Figure 5), only subclonal variants from pyclone clusters present in phylogenetic trees
756 were displayed, this did not affect ctDNA detection status of any time-points. In non-relapse
757 cases presented in Extended Data Fig 6 all detected subclonal SNVs were plotted. To determine
758 the relationship between tumor volume and ctDNA VAF, ctDNA assays against clonal SNVs
759 were selected. For each patient, the mean ctDNA VAF of the clonal SNVs was determined as
760 baseline for 38/46 patients with at least 2 SNVs detected in plasma. As detailed in Extended
761 Fig. 4c, 8/46 patients were not included in the analysis: CRUK0036 had no pre-op CT scan
762 available, CRUK0087 had a large cavity inside the primary cancer, CRUK0099 had a collapsed
763 lung making volume assessment inaccurate, CRUK0100, CRUK0077, CRUK0052 had a CT
764 slice spacing of > 5 mm, and finally CRUK0088 and CRUK0091 had a total tumor volume <
765 3.5 cm^3. Linear regression was performed on log-transformed mean VAF and tumor volume.
766 The log transformation was justified as it symmetrized the residuals in the model. An
767 independent analysis was performed where tumor volume was multiplied with tumor purity to
768 estimate the cancer cell volume. The same log transformation and analysis was applied to data

769 acquired from Newman et al.[16], where ctDNA VAF was determined based on CAPP-seq
770 analysis with matched tumor volume data available. To analyze clone size versus ctDNA VAF
771 for subclonal SNVs, the mean CCF of the mutations within a subclonal mutation cluster was
772 multiplied with tumor volume, and as a second independent analysis, with tumor purity.

773 **Method References**

774 24. Hofheinz F, Butof R, Apostolova I, Zophel K, Steffen IG, Amthauer H, et al. An
775 investigation of the relation between tumor-to-liver ratio (TLR) and tumor-to-blood
776 standard uptake ratio (SUR) in oncological FDG PET. EJNMMI Res 2016;6(1):19.
777 25. Butof R, Hofheinz F, Zophel K, Stadelmann T, Schmollack J, Jentsch C, et al.
778 Prognostic Value of Pretherapeutic Tumor-to-Blood Standardized Uptake Ratio in
779 Patients with Esophageal Carcinoma. J Nucl Med 2015;56(8):1150-6.
780 26. Malikic S, McPherson AW, Donmez N, Sahinalp CS. Clonality inference in multiple
781 tumor samples using phylogeny. Bioinformatics 2015;31(9):1349-56.
782 27. Lappalainen I, Almeida-King J, Kumanduri V, Senf A, Spalding JD, Ur-Rehman S, et
783 al. The European Genome-phenome Archive of human data consented for biomedical
784 research. Nat Genet 2015;47(7):692-5.

Data availability Statement

Sequence data has been deposited at the European Genome-Phenoma Archive (EGA), which is hosted by the The European Bioinformatics Institute (EBI) and the Centre for Genomic Regulation (CRG), under accession numbers EGAS00001002247 (primary tumor data) and EGAS00001002415 (metastatic tumor data). Further information about EGA can be found on https://ega-archive.org, "The European Genome-phenome Archive of human data consented for biomedical research"[27].

Extended Figure Legends

Extended Data Figure 1. Multiplex-PCR next-generation sequencing platform analytical validation

a) Analytical validation of the multiplex-PCR NGS platform was performed by spiking synthetic single nucleotide variants into control cell-free DNA. Sensitivity and specificity of the platform at different spike concentrations was ascertained, 95% binomial confidence interval displayed as error bars. b) Specificity of ctDNA detection based on a 1 SNV and 2 SNV call threshold taking into account parallel testing of multiple SNVs. c) The median depth of read across a position did not vary depending on whether an SNV position was called or not

called using the platform error-model. Wilcoxon Test, P=0.786, median depth of read at uncalled positions = 45,777 (n=3,745), range: 0 to 146774, median depth of read at called positions = 45,478, range= 1,354 to 152,974 (n=1,124). Whiskers represent 1.5 times the interquartile range, 2-sided test.

Extended Data Figure 2. Study construction and assay-panel design

a) The pre-operative study phase cohort consisted of 100 TRACERx patients present in the first 100 patient TRACERx cohort in April 2016. Pre-operative plasma samples were profiled in 96 patients for reasons listed. bi and ii) Contents of patient-specific assay-panels designed in the pre-operative study phase. c) The longitudinal study phase cohort consisted of patients with confirmed NSCLC relapse and patients without relapse. d) Contents of patient-specific assay-panels designed in the longitudinal phases of this study. e) Single nucleotide variant type targeted.

Extended Data Figure 3 – Clinicopathological predictors of ctDNA detection

a) 96 patients in pre-operative cohort stratified by pathological TNM stage. b) LUSCs and ctDNA positive LUADs are significantly more necrotic that ctDNA negative LUADs. Significant differences in necrosis between groups: LUSCs (median necrosis 40%) (n=31), ctDNA positive LUADs (median necrosis 15%) (n=11) and ctDNA negative LUADs (median necrosis 2%) (n=47), Kruskal-Wallis test, $P<0.001$, 2-sided pairwise comparisons were performed using Dunn's procedure with Bonferroni correction. c) Univariate (left) and multivariate analyses (right) were performed, by logistic regression to determine significant predictors of ctDNA detection in early-stage NSCLC. ctDNA detection was defined as detection of two or more SNVs in pre-operative plasma samples. Details regarding multivariable analysis methodology are in methods. d) Receiver operating characteristic curve (ROC) analysis of pre-operative PET scan FDG-avidity (normalized as tumor background ratio (TBR), see methods), as a predictor of ctDNA detection (92/96 PET scans were available for central review). Median PET TBR of detected tumors = 9.01, n=45. Median PET TBR of undetected tumors= 3.64, n=47. P-value based on Wilcoxon Rank Sum Test. e) LUAD subtype analyses based on ctDNA detection and the presence of an EGFR, KRAS or TP53 driver mutation.

Extended Data Figure 4. Predictors of plasma variant allele frequency

a) Plasma variant allele frequencies of SNVs detected in plasma in 46 patients who were ctDNA positive (two or more SNVs detected). Clonal (blue) and subclonal (red) variant allele frequencies indicated, mean shown as horizontal line. Driver variants shown as triangles. b) Mean clonal VAF correlated with maximum tumor size measured in post-surgical specimen (pathological size, n=46) grey vertical bars represent range of clonal variant allele frequency. Shaded red background indicates 95% confidence interval. c) Filtering steps taken to define a group of ctDNA positive patients with volumetric data considered adequate to model tumor volume and plasma variant allele frequency. d) Scatter plot showing mean clonal VAF relative to tumor volume for TRACERx (blue dots and fitted blue line, n=38) and VAF relative to volume for previously published data based on CAPP-seq analysis of ctDNA (orange dots and orange fitted line, n=9). Orange shaded background indicates 95% confidence interval based on CAPP-seq data. e) Mean clonal VAF correlated with tumor volume × tumor purity (cancer cell volume), n=38. Shaded red background indicates 95% confidence interval. f) Association between number of cancer cells and VAF of clonal SNVs in plasma based on linear modelling of Extended Data Fig 4f. g) Detected subclonal SNVs were mapped back to M-Seq derived tumor phylogenetic trees (process illustrated in

graphic). Detected private subclones (subclones identified within only a single tumor region) are coloured red. Shared subclones (subclones detected in more than one tumor regions) are light blue. Subclonal nodes were sized based on the maximum recorded cancer cell fraction (CCF). The top row of phylogenetic trees represent subclonal nodes targeted by primers within that patient's assay panel, the bottom row represent subclonal nodes detected in ctDNA, within this row grey subclonal nodes represent subclones not detected in ctDNA.

Extended Data Figure 5. Longitudinal ctDNA profiling, remaining relapse cases. a) Kaplan-Meier curve demonstrate relapse free survival for patients in whom ctDNA was detected versus patients in whom ctDNA was not detected. b-h) Longitudinal cell-free DNA profiling. Circulating tumor DNA (ctDNA) detection in plasma was defined as the detection of two tumor-specific SNVs. Relapse was based on imaging-confirmed NSCLC relapse, imaging performed as clinically indicated. Detected clonal (circles, light blue) and subclonal (triangles, colors indicates different subclones) SNVs from each patient-specific assay-panel are plotted on graphs colored by M-Seq derived tumor phylogenetic nodes. Mean clonal (blue) and mean subclonal (red) VAF are indicated on graphs. Pre-operative and relapse M-

Seq derived phylogenetic trees represented by ctDNA are illustrated above each graph in cases where subclonal SNVs were detected.

Extended Data Figure 6. Longitudinal ctDNA profiling, non-relapse cases a-j) Detected clonal (circles, light blue) and subclonal (red triangles) SNVs from each patient-specific assay-panel are plotted on graphs. Mean clonal (blue) and mean subclonal (red) VAF are indicated on graphs.

Extended Data Figure 7. Heatmaps illustrating detection of SNVs in bespoke panel at each sampled time point a, c-f) Bespoke assay panels for CRUK0063, CRUK0035, CRUK0044, CRUK0041 and CRUK0013. Colors indicate originating subclonal cluster based on the phylogenetic trees above the heatmap. Light blue indicates clonal mutation cluster. Full panel with cluster color shown below each heatmap. Filled squares indicates detection of a given variant in plasma ctDNA. Y-axis shows day of sampling, y-axis labels appended with [R] indicates day of clinical relapse. b) Re-examination of primary tumor regions from CRUK0063 with lowered threshold to potentially identify SNVs private to the sequenced

relapse biopsy. 16/88 variants were found at very low VAF in region 3, indicating this region from the primary likely gave rise to the metastasis.

Extended Data Figure 8. Heatmap illustrating detection of SNVs in bespoke panel based on M-seq of metastatic tumor regions for patient CRUK0063 for all sampled time points. Colors indicate originating subclonal cluster based on the phylogenetic trees above the heatmap. Light blue indicates clonal mutation cluster. Full panel with cluster color shown below each heatmap. Filled squares indicates detection of a given variant in plasma ctDNA. Y-axis shows day of sampling.

Extended Table 1. Patient characteristics a) table of clinical characteristics describing the 96 patient pre-operative cohort and b) demonstrating distribution of stage and whether the patient received adjuvant chemotherapy, c) demonstrating the time-points at which pre-operative plasma was acquired for patients within the cohort, d) table of clinical characteristics describing 24 patient longitudinal cohort and e) demonstrating distribution of stage in the longitudinal cohort and whether the patient received adjuvant chemotherapy.

Extended Table 2. Cross platform validation using a generic approach to ctDNA profiling

a) 7/10 (70%) of bespoke-panel ctDNA positive patients had tumor SNVs detectable in plasma preoperatively by a generic hotspot PCR-NGS lung panel (Lung Oncomine, Thermofisher). The three bespoke-panel ctDNA positive patients undetected by the generic panel had mean clonal plasma variant allele frequencies lower than the 0.1% plasma variant allele frequency (VAF) limit of detection reported for the generic panel (shaded yellow**).** b) Based on CT volumetric assessment of each patient's primary tumor we predicted plasma VAF corresponding to a tumor of that size (see Figure 3 and Methods for details of approach). This allowed us to infer platform sensitivities for each patient within the bespoke-panel non-detected cohort. Five LUADs (shaded green, CRUK0037, CRUK0051, CRUK0004, CRUK0039 and CRUK0025) had tumor volumes approximating to a plasma VAF of more than 0.1%. This suggested that these tumors resided within the top platform sensitivity bracket of both the generic and bespoke-panel ctDNA platforms. No ctDNA was detected by either platform in these cases, suggesting biological specificity of the bespoke-panel. c) Hotspot SNVs not identified in tumor tissue through exome sequencing were identified in plasma of 9 of 28 patients by the generic panel. This suggested non-tumor origin of cell-free DNA, platform non-specificity or an evolving minor subclone or second primary.

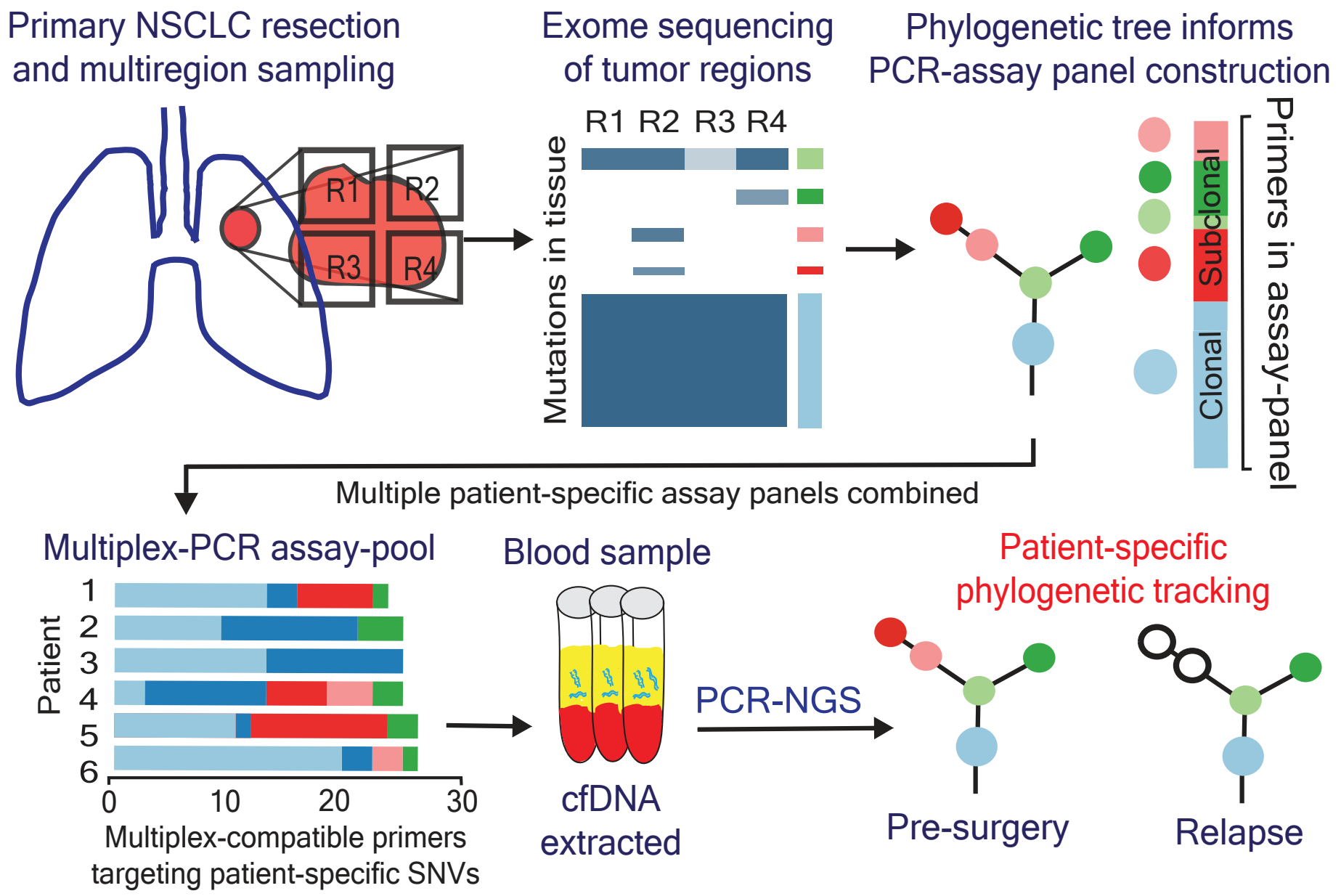
Primary NSCLC resection and multiregion sampling
R1
R2
R3
R4
Exome sequencing of tumor regions
R1 R2 R3 R4
Mutations in tissue
Phylogenetic tree informs PCR-assay panel construction
Subclonal
Clonal
Primers in assay-panel
Multiple patient-specific assay panels combined
Multiplex-PCR assay-pool
Patient
1
2
3
4
5
6
0
10
20
30
Multiplex-compatible primers targeting patient-specific SNVs
Blood sample
cfDNA extracted
PCR-NGS
Patient-specific phylogenetic tracking
Pre-surgery
Relapse

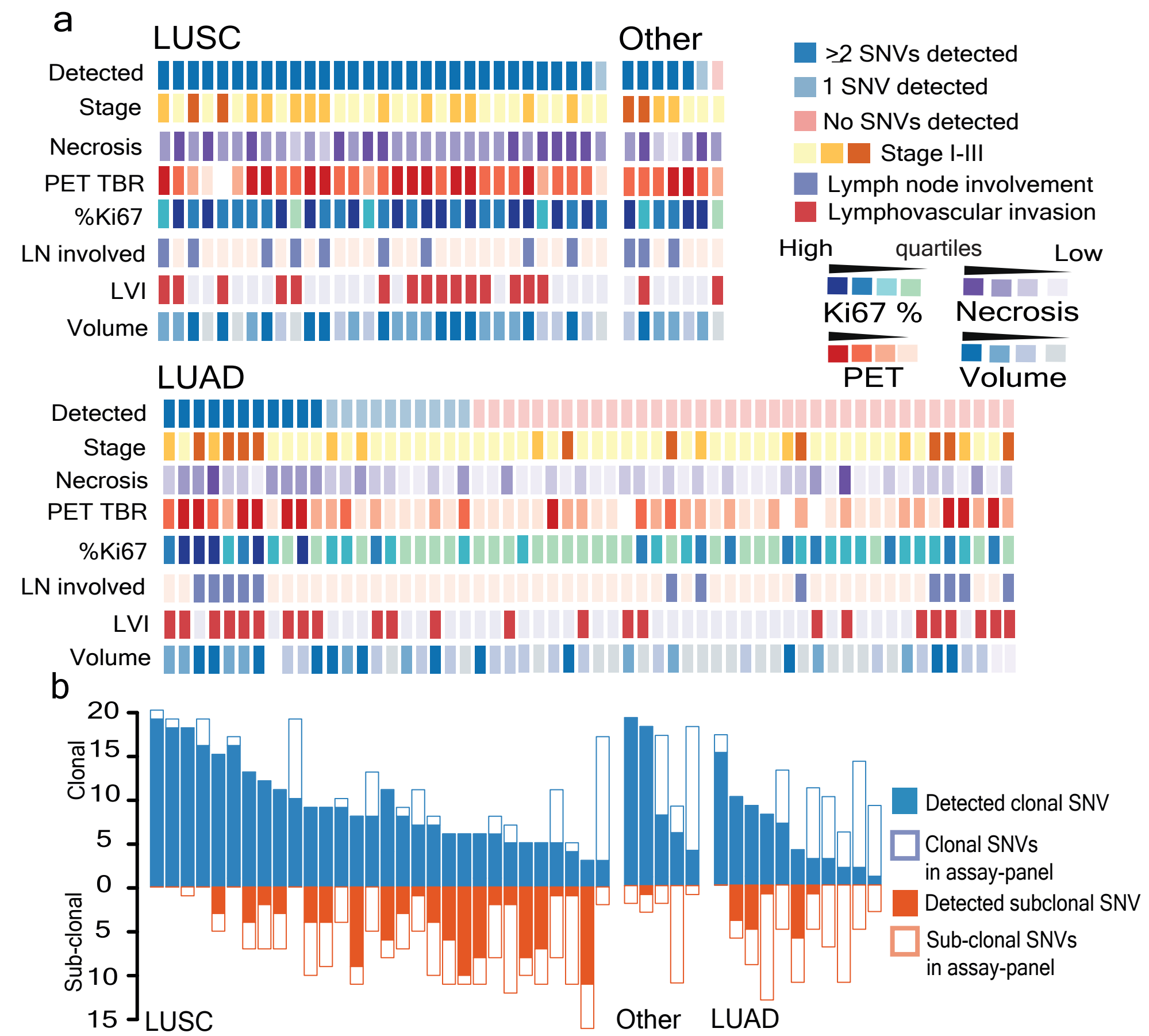
a
LUSC
Other
Detected
Stage
Necrosis
PET TBR
%Ki67
LN involved
LVI
Volume
≥2 SNVs detected
1 SNV detected
No SNVs detected
Stage I-III
Lymph node involvement
Lymphovascular invasion
High
quartiles
Low
Ki67 %
Necrosis
PET
Volume
LUAD
Detected
Stage
Necrosis
PET TBR
%Ki67
LN involved
LVI
Volume
b
20
15
10
5
0
5
10
15
Clonal
Sub-clonal
LUSC
Other
LUAD
Detected clonal SNV
Clonal SNVs in assay-panel
Detected subclonal SNV
Sub-clonal SNVs in assay-panel

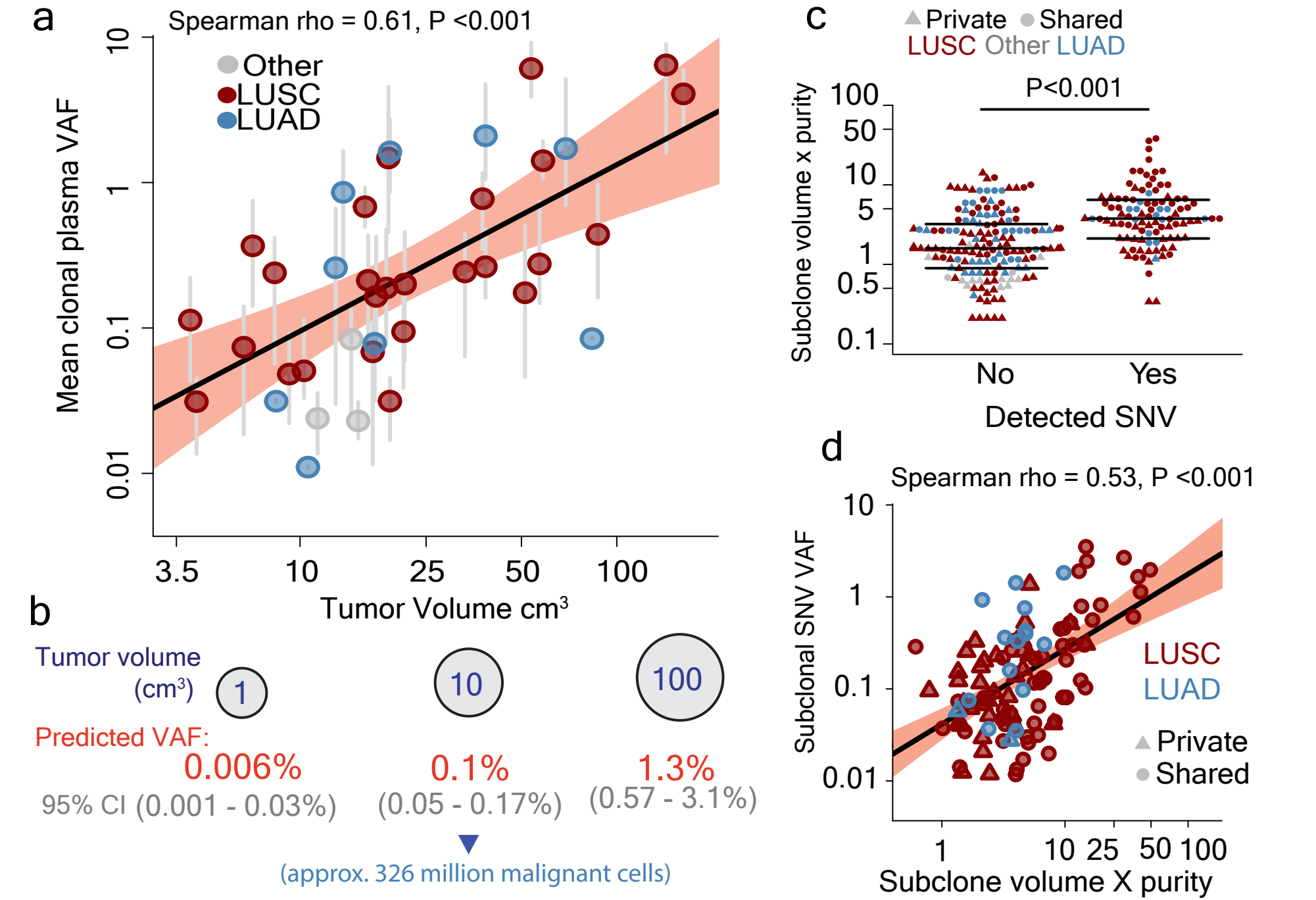
a
Spearman rho = 0.61, P <0.001
Other
LUSC
LUAD
Mean clonal plasma VAF
10
1
0.1
0.01
3.5
10
25
50
100
Tumor Volume cm3
b
Tumor volume (cm3)
1
10
100
Predicted VAF:
0.006%
95% CI (0.001 - 0.03%)
0.1%
(0.05 - 0.17%)
1.3%
(0.57 - 3.1%)
(approx. 326 million malignant cells)
c
Private
Shared
LUSC Other LUAD
P<0.001
Subclone volume x purity
100
50
10
5
1
0.5
0.1
No
Yes
Detected SNV
d
Spearman rho = 0.53, P <0.001
Subclonal SNV VAF
10
1
0.1
0.01
LUSC
LUAD
Private
Shared
1
10
25
50
100
Subclone volume X purity

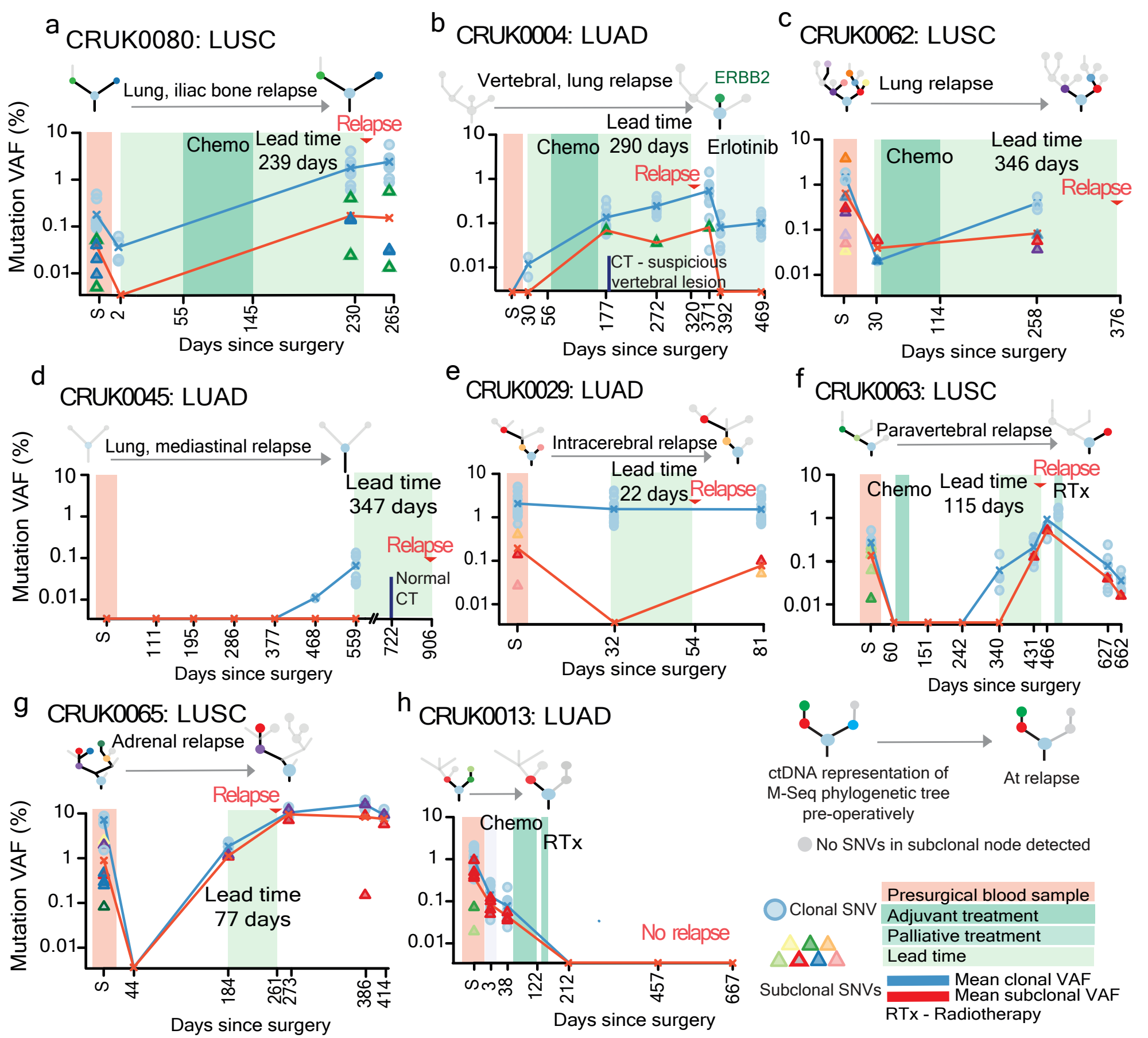
a
CRUK0080: LUSC
Lung, iliac bone relapse
Relapse
Chemo
Lead time
239 days
Mutation VAF (%)
10
1
0.1
0.01
S
2
55
145
230
265
Days since surgery
b
CRUK0004: LUAD
Vertebral, lung relapse
ERBB2
Lead time
290 days
Chemo
Erlotinib
Relapse
CT - suspicious
vertebral lesion
S
30
56
177
272
320
371
392
469
Days since surgery
c
CRUK0062: LUSC
Lung relapse
Chemo
Lead time
346 days
Relapse
S
30
114
258
376
Days since surgery
d
CRUK0045: LUAD
Lung, mediastinal relapse
Lead time
347 days
Relapse
Normal
CT
S
111
195
286
377
468
559
722
906
Days since surgery
e
CRUK0029: LUAD
Intracerebral relapse
Lead time
22 days
Relapse
S
32
54
81
Days since surgery
f
CRUK0063: LUSC
Paravertebral relapse
Chemo
Lead time
115 days
Relapse
RTx
S
60
151
242
340
431
466
627
662
Days since surgery
g
CRUK0065: LUSC
Adrenal relapse
Relapse
Lead time
77 days
S
44
184
261
273
386
414
Days since surgery
h
CRUK0013: LUAD
Chemo
RTx
No relapse
S
3
38
122
212
457
667
Days since surgery
ctDNA representation of
M-Seq phylogenetic tree
pre-operatively
At relapse
No SNVs in subclonal node detected
Clonal SNV
Subclonal SNVs
Presurgical blood sample
Adjuvant treatment
Palliative treatment
Lead time
Mean clonal VAF
Mean subclonal VAF
RTx - Radiotherapy

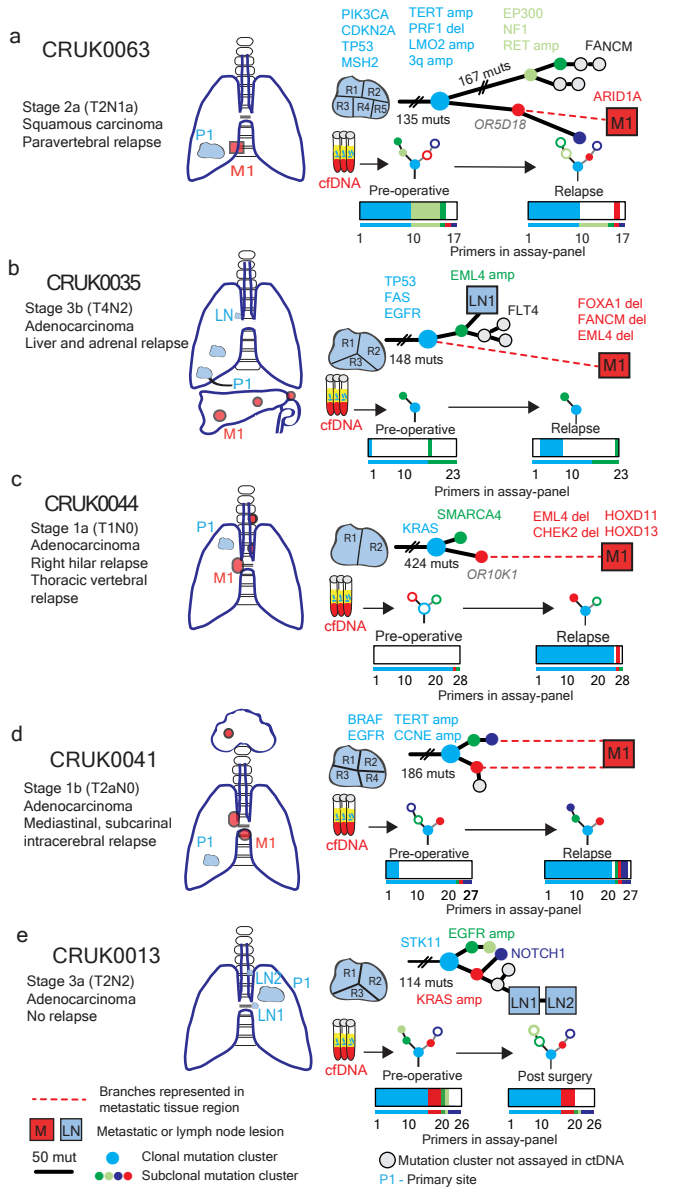
a
CRUK0063
Stage 2a (T2N1a)
Squamous carcinoma
Paravertebral relapse
P1
M1
PIK3CA
CDKN2A
TP53
MSH2
TERT amp
PRF1 del
LMO2 amp
3q amp
EP300
NF1
RET amp
FANCM
167 muts
ARID1A
135 muts
OR5D18
M1
R1
R2
R3
R4
R5
cfDNA
Pre-operative
Relapse
1
10
17
Primers in assay-panel
b
CRUK0035
Stage 3b (T4N2)
Adenocarcinoma
Liver and adrenal relapse
LN1
P1
M1
TP53
FAS
EGFR
EML4 amp
FLT4
FOXA1 del
FANCM del
EML4 del
148 muts
23
c
CRUK0044
Stage 1a (T1N0)
Adenocarcinoma
Right hilar relapse
Thoracic vertebral relapse
KRAS
SMARCA4
EML4 del
CHEK2 del
HOXD11
HOXD13
424 muts
OR10K1
28
d
CRUK0041
Stage 1b (T2aN0)
Adenocarcinoma
Mediastinal, subcarinal
intracerebral relapse
BRAF
EGFR
TERT amp
CCNE amp
186 muts
27
e
CRUK0013
Stage 3a (T2N2)
Adenocarcinoma
No relapse
LN2
LN1
STK11
EGFR amp
NOTCH1
114 muts
KRAS amp
26
Post surgery
Branches represented in metastatic tissue region
Metastatic or lymph node lesion
50 mut
Clonal mutation cluster
Subclonal mutation cluster
Mutation cluster not assayed in ctDNA
P1 - Primary site

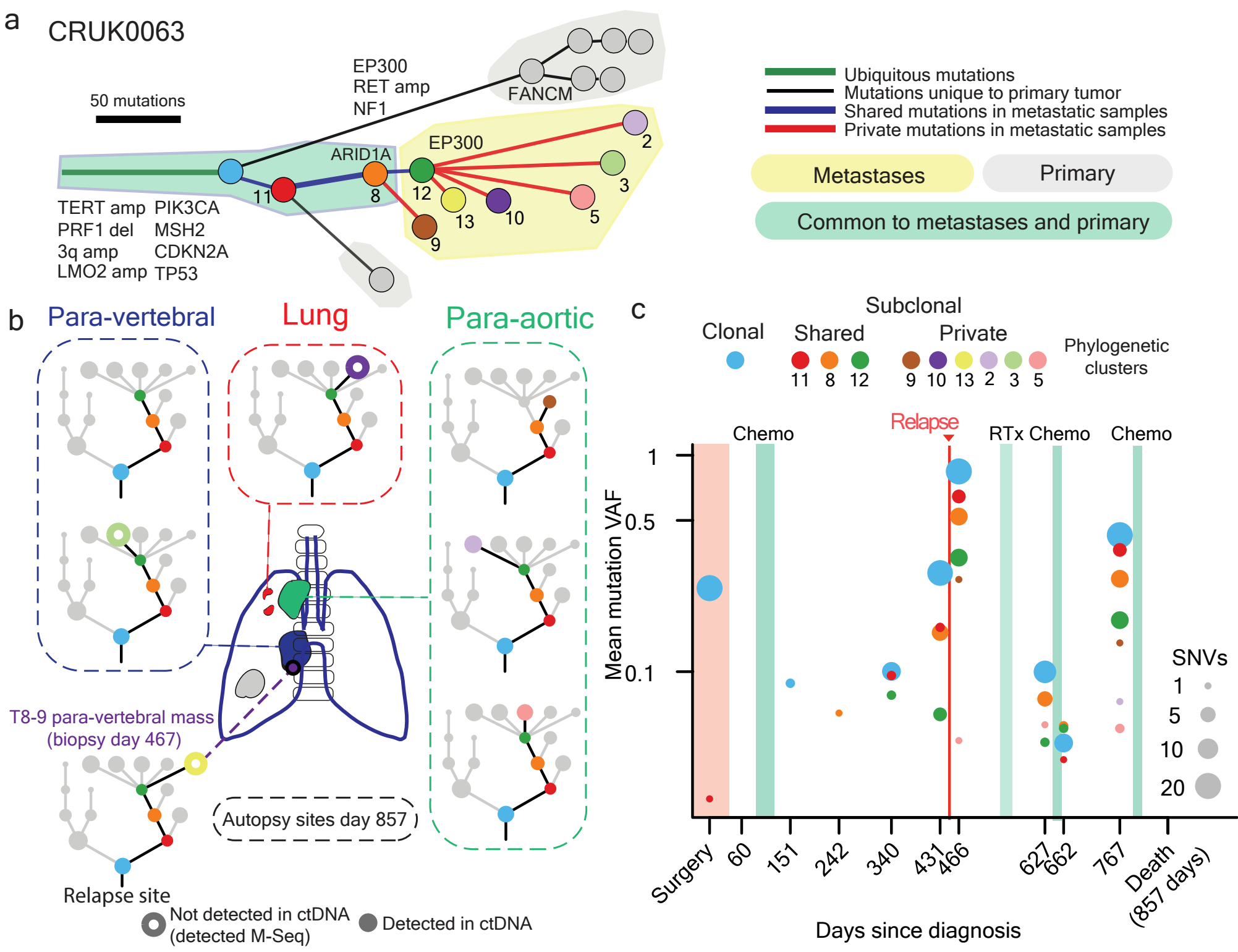
a
CRUK0063
50 mutations
EP300
RET amp
NF1
FANCM
ARID1A
EP300
TERT amp
PRF1 del
3q amp
LMO2 amp
PIK3CA
MSH2
CDKN2A
TP53
11
8
12
13
10
9
2
3
5
Ubiquitous mutations
Mutations unique to primary tumor
Shared mutations in metastatic samples
Private mutations in metastatic samples
Metastases
Primary
Common to metastases and primary
b
Para-vertebral
Lung
Para-aortic
T8-9 para-vertebral mass
(biopsy day 467)
Autopsy sites day 857
Relapse site
Not detected in ctDNA
(detected M-Seq)
Detected in ctDNA
c
Subclonal
Clonal
Shared
Private
11 8 12
9 10 13 2 3 5
Phylogenetic
clusters
Chemo
Relapse
RTx Chemo
Chemo
Mean mutation VAF
1
0.5
0.1
SNVs
1
5
10
20
Surgery
60
151
242
340
431
466
627
662
767
Death
(857 days)
Days since diagnosis

a Multiplex-PCR platform sensitivity and specificity

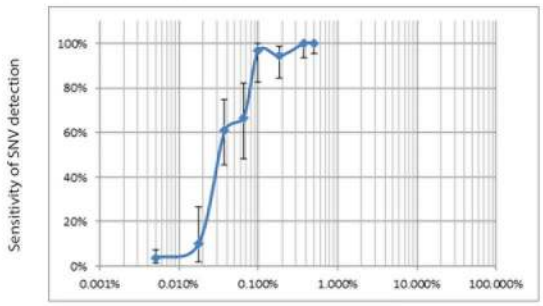

SNV spike input range	Eligible positive positions	True positive calls	Sensitivity	95% CI
>0.5	81	81	100.0%	95.6-100%
0.25-0.5%	54	54	100.0%	93.4-100%
0.1-0.25%	66	64	97.0%	89.5-99.6%
0.05-0.1%	51	43	84.3%	71.4-93.0%
0.01-0.05%	76	35	46.1%	34.6-57.9%
<=0.01%	212	9	4.2%	2-7.8%
	Eligible negative positions	**False positive calls**	**Specificity**	**95% CI**
	5099	19	99.6%	99.4-99.8%

b

SNVs tested for in ctDNA per patient	Predicted specificity for ctDNA detection: 1 SNV threshold	2 SNV threshold
1	99.63%	
5	98.16%	99.99%
10	96.36%	99.94%
20	92.85%	99.75%
30	89.48%	99.44%
50	83.08%	98.51%
100	69.03%	94.66%
200	47.65%	83.04%

2 SNV threshold caclulated based on binomial probability using false positive rate of 0.0037.

c

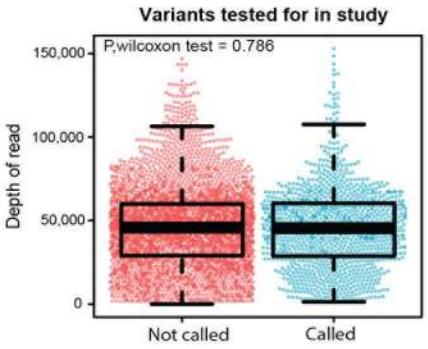

a

Pre-operative study phase cohort design

TRACERx cohort April 2016 (n=100)

Excluded
CRUK0092- no pre-operative blood sample donated

Exome analysis pipeline (n=99)

Excluded
CRUK0136 and CRUK0129 - failed bioinformatic quality control of whole exome sequencing data

Multiplex-PCR NGS platform (n=97)

Excluded
CRUK0060 - failed multiplex-PCR platform

Pre-operative study phase cohort (n=96)

b

Pre-operative study phase assay-panel design

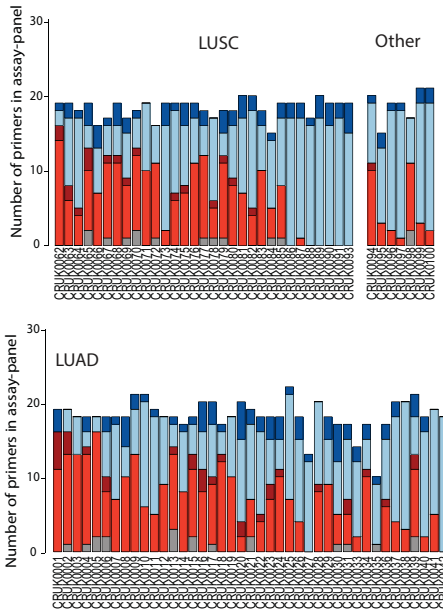

c

Longitudinal study phase cohort design

TRACERx cohort April 2016 (n=100)

15 confirmed NSCLC relapses in cohort

Excluded
CRUK0077 and CRUK0003 - insufficient post-operative blood donated
CRUK0094 - Withdrawn due to ill-health, no relapse blood donated

12 non-relapse patients selected
- No clinical evidence of NSCLC relapse,
- Multiple post-operative plasma samples of sufficient volume

NSCLC relapse reported in control case
CRUK0021 - May 2016
CRUK0045 - December 2016

Longitudinal cohort contains 10 control cases and 14 confirmed NSCLC relapses (n=24)

d

Longitudinal study phase assay-panel design

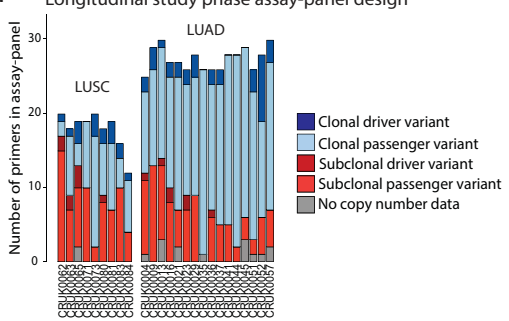

e

SNV type targeted	Pre -operative assay -panels	Longitudinal assay -panels
Non -synonymous	1,547	542
Stopgain	155	50
Stop loss	1	10
Synonymous	44	0
Unknown	1	0
Total	1,748	602

a

Histological subtype			TNM Stage I	II	III	Total
LUAD	ctDNA detected	Yes	5	2	4	11
		No	34	7	6	47
LUSC	ctDNA detected	Yes	16	12	2	30
		No	1	0	0	1
Other	ctDNA detected	Yes	1	2	2	5
		No	2	0	0	2

b

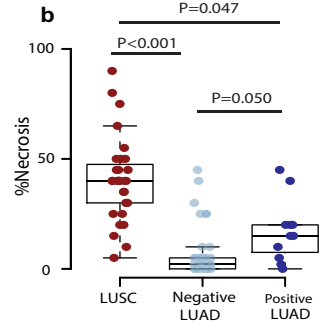

c

Predictors of ctDNA detection by multiplex-PCR NGS in early stage NSCLC

	Univariable analysis		Multivariable analysis	
	OR (95% CI)	P-value	OR (95% CI)	P-value
Clinicopathological variables				
Non-adenocarcinoma histology	49.85 (12.93 -192.19)	<0.001	40.76 (4.55 - 365.14)	0.001
%Ki67^{+} cells (10% increase)	1.72 (1.40 - 2.12)	<0.001	1.40 (1.05 - 1.84)	0.022
Lympho-vascular invasion	2.53 (1.10 - 5.80)	0.028	5.84 (1.07 - 32.03)	0.042
Necrosis (10% increase)	2.16 (1.58 - 2.97)	<0.001	1.04 (0.64 - 1.71)	0.862
Path tumour size (10mm increase)	1.45 (1.13 - 1.86)	0.004	1.32 (0.91-1.91)	0.134
Lymph-node involvement	3.60 (1.33 - 9.77)	0.012	3.82 (0.61 - 23.99)	0.153
Male gender	1.80 (0.78 - 4.16)	0.172	1.06 (0.21-5.39)	0.941
Age (years)	0.96 (0.92 - 1.01)	0.115	0.99 (0.92-1.07)	0.820
Technical variables				
cfDNA input (ng)	1.01 (1.00 - 1.03)	0.028	1.01 (1.00 - 1.02)	0.229
Ubiquitous SNVs in assay-panel	0.96 (0.88 - 1.05)	0.341	1.00 (0.84 - 1.19)	0.975

Ubiquitous SNVs (SNVs present in all tumour regions sequenced).

d

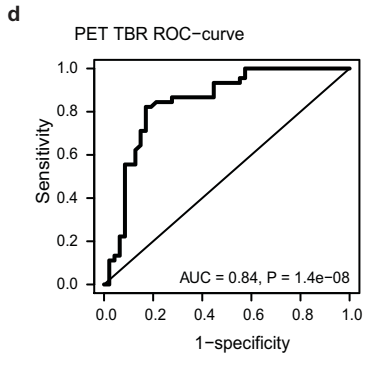

e

LUAD

		TP53 driver Yes	No	Total
ctDNA detected	Yes	4	7	11
	No	24	23	47
Total		28	30	58

Fishers Exact Test P=0.508

		KRAS driver Yes	No	Total
ctDNA detected	Yes	3	8	11
	No	20	27	47
Total		23	35	58

Fishers Exact Test P=0.499

		EGFR driver Yes	No	Total
ctDNA detected	Yes	1	10	11
	No	11	36	47
Total		12	46	58

Fishers Exact Test P=0.429

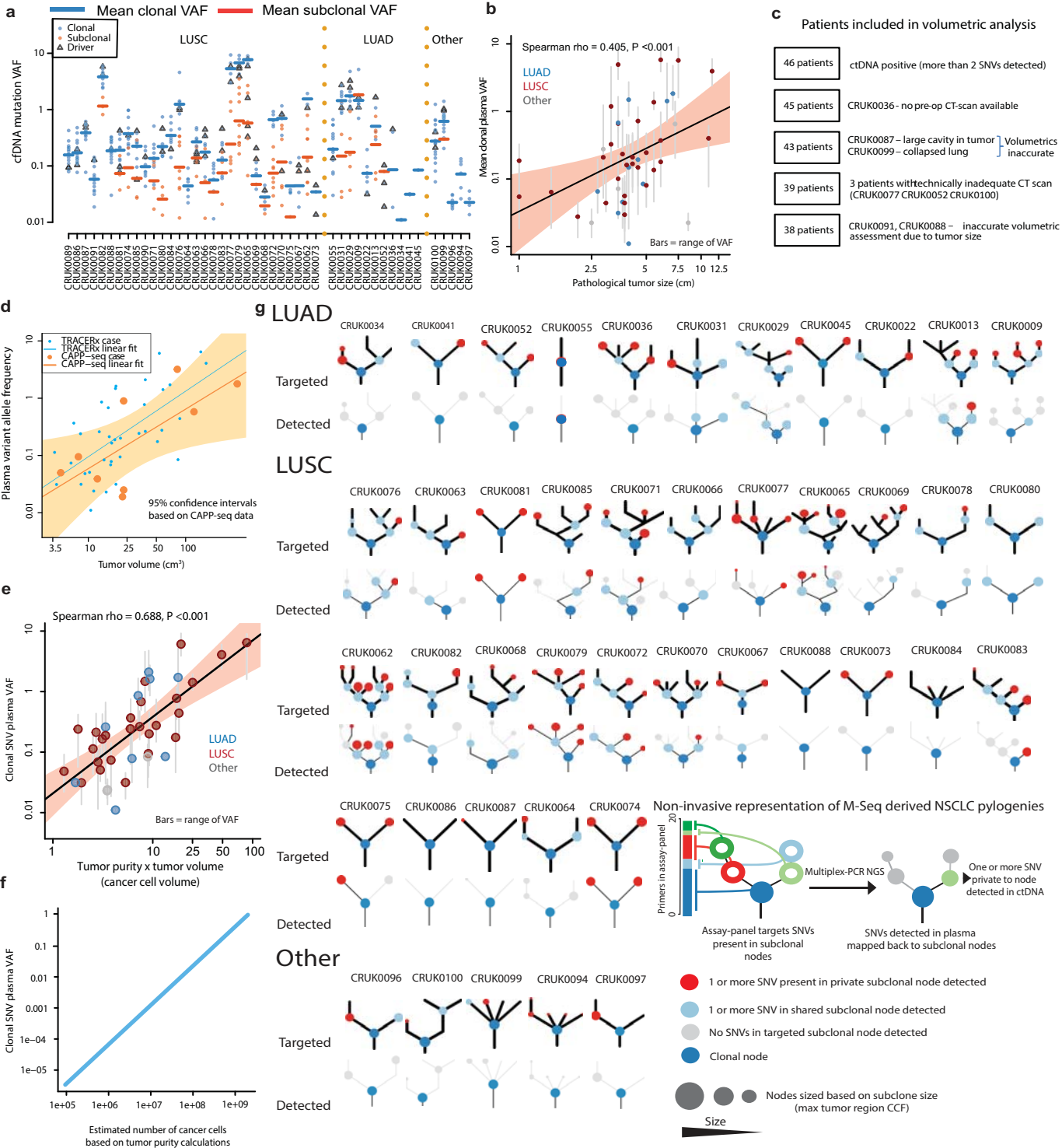
a
Mean clonal VAF
Mean subclonal VAF
Clonal
Subclonal
Driver
LUSC
LUAD
Other
cfDNA mutation VAF
b
Spearman rho = 0.405, P <0.001
LUAD
LUSC
Other
Mean clonal plasma VAF
Bars = range of VAF
Pathological tumor size (cm)
c
Patients included in volumetric analysis
46 patients
ctDNA positive (more than 2 SNVs detected)
45 patients
CRUK0036 - no pre-op CT-scan available
43 patients
CRUK0087 – large cavity in tumor
CRUK0099 – collapsed lung
Volumetrics inaccurate
39 patients
3 patients with technically inadequate CT scan (CRUK0077 CRUK0052 CRUK0100)
38 patients
CRUK0091, CRUK0088 – inaccurate volumetric assessment due to tumor size
d
TRACERx case
TRACERx linear fit
CAPP–seq case
CAPP–seq linear fit
Plasma variant allele frequency
95% confidence intervals based on CAPP-seq data
Tumor volume (cm³)
e
Spearman rho = 0.688, P <0.001
Clonal SNV plasma VAF
LUAD
LUSC
Other
Bars = range of VAF
Tumor purity x tumor volume (cancer cell volume)
f
Clonal SNV plasma VAF
Estimated number of cancer cells based on tumor purity calculations
g
LUAD
CRUK0034
CRUK0041
CRUK0052
CRUK0055
CRUK0036
CRUK0031
CRUK0029
CRUK0045
CRUK0022
CRUK0013
CRUK0009
Targeted
Detected
LUSC
CRUK0076
CRUK0063
CRUK0081
CRUK0085
CRUK0071
CRUK0066
CRUK0077
CRUK0065
CRUK0069
CRUK0078
CRUK0080
CRUK0062
CRUK0082
CRUK0068
CRUK0079
CRUK0072
CRUK0070
CRUK0067
CRUK0088
CRUK0073
CRUK0084
CRUK0083
CRUK0075
CRUK0086
CRUK0087
CRUK0064
CRUK0074
Non-invasive representation of M-Seq derived NSCLC pylogenies
Primers in assay-panel
Multiplex-PCR NGS
One or more SNV private to node detected in ctDNA
Assay-panel targets SNVs present in subclonal nodes
SNVs detected in plasma mapped back to subclonal nodes
Other
CRUK0096
CRUK0100
CRUK0099
CRUK0094
CRUK0097
1 or more SNV present in private subclonal node detected
1 or more SNV in shared subclonal node detected
No SNVs in targeted subclonal node detected
Clonal node
Nodes sized based on subclone size (max tumor region CCF)
Size

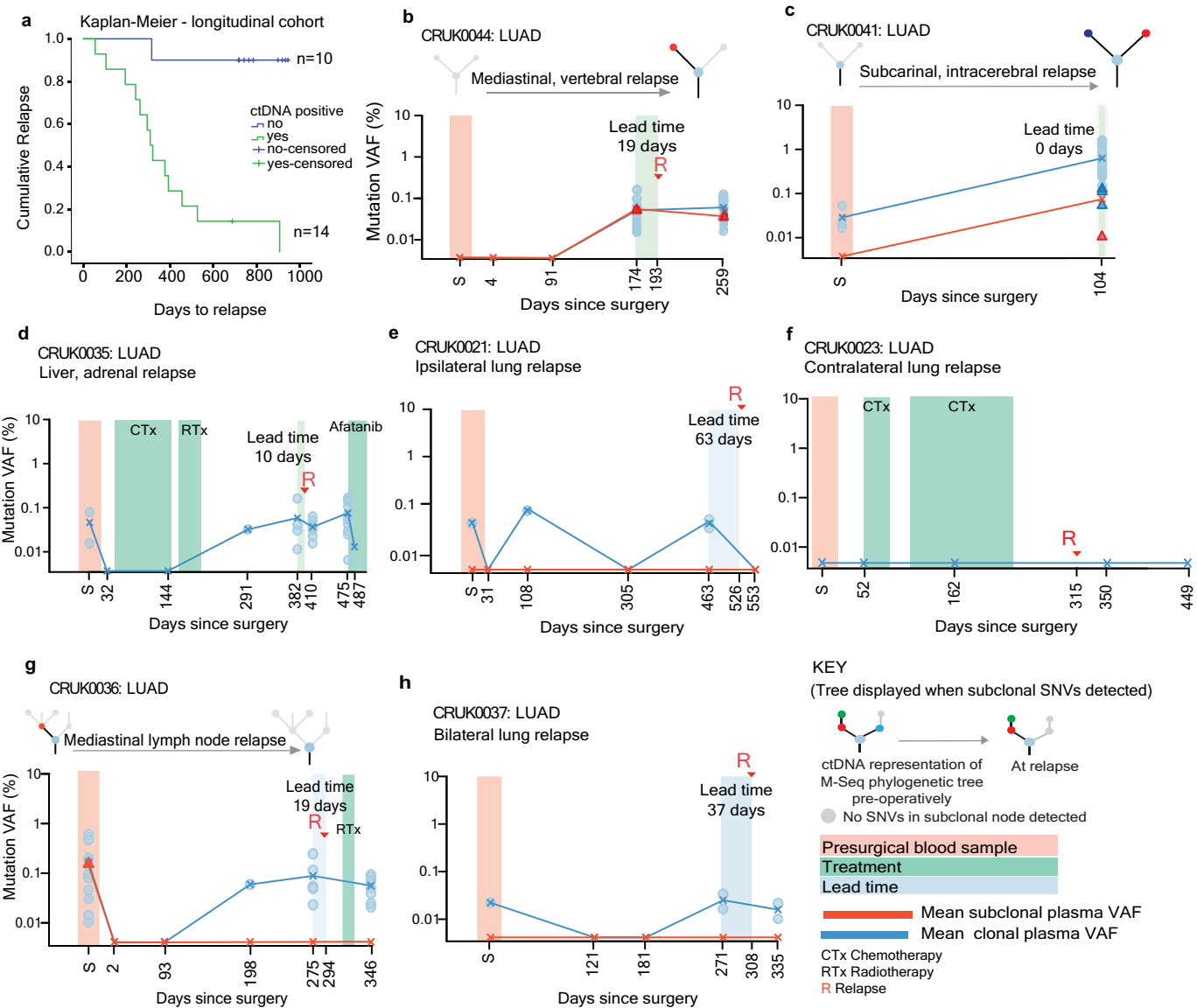
a
Kaplan-Meier - longitudinal cohort
Cumulative Relapse
Days to relapse
ctDNA positive
no
yes
no-censored
yes-censored
n=10
n=14
b
CRUK0044: LUAD
Mediastinal, vertebral relapse
Mutation VAF (%)
Lead time
19 days
R
Days since surgery
c
CRUK0041: LUAD
Subcarinal, intracerebral relapse
Lead time
0 days
Days since surgery
d
CRUK0035: LUAD
Liver, adrenal relapse
CTx
RTx
Afatanib
Lead time
10 days
Mutation VAF (%)
Days since surgery
e
CRUK0021: LUAD
Ipsilateral lung relapse
Lead time
63 days
Days since surgery
f
CRUK0023: LUAD
Contralateral lung relapse
CTx
CTx
Days since surgery
g
CRUK0036: LUAD
Mediastinal lymph node relapse
Lead time
19 days
RTx
Mutation VAF (%)
Days since surgery
h
CRUK0037: LUAD
Bilateral lung relapse
Lead time
37 days
Days since surgery
KEY
(Tree displayed when subclonal SNVs detected)
ctDNA representation of
M-Seq phylogenetic tree
pre-operatively
At relapse
No SNVs in subclonal node detected
Presurgical blood sample
Treatment
Lead time
Mean subclonal plasma VAF
Mean clonal plasma VAF
CTx Chemotherapy
RTx Radiotherapy
R Relapse

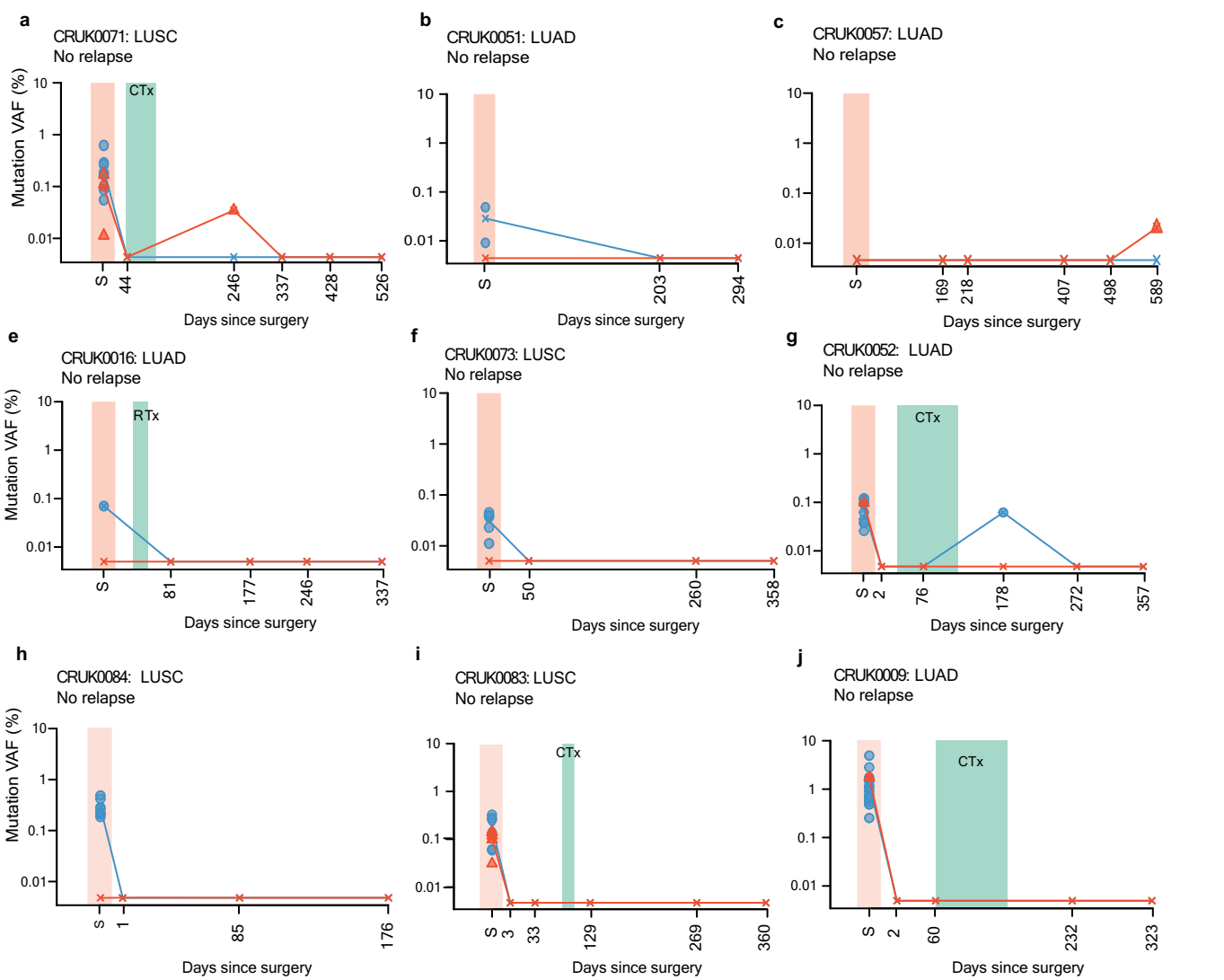
a
CRUK0071: LUSC
No relapse
CTx
Mutation VAF (%)
10
1
0.1
0.01
S
44
246
337
428
526
Days since surgery
b
CRUK0051: LUAD
No relapse
S
203
294
Days since surgery
c
CRUK0057: LUAD
No relapse
S
169
218
407
498
589
Days since surgery
e
CRUK0016: LUAD
No relapse
RTx
S
81
177
246
337
Days since surgery
f
CRUK0073: LUSC
No relapse
S
50
260
358
Days since surgery
g
CRUK0052: LUAD
No relapse
CTx
S
2
76
178
272
357
Days since surgery
h
CRUK0084: LUSC
No relapse
S
1
85
176
Days since surgery
i
CRUK0083: LUSC
No relapse
CTx
S
3
33
129
269
360
Days since surgery
j
CRUK0009: LUAD
No relapse
CTx
S
2
60
232
323
Days since surgery
KEY
Presurgical blood sample
Adjuvant treatment
Mean subclonal plasma VAF
Mean clonal plasma VAF
CTx Chemotherapy
RTx Radiotherapy

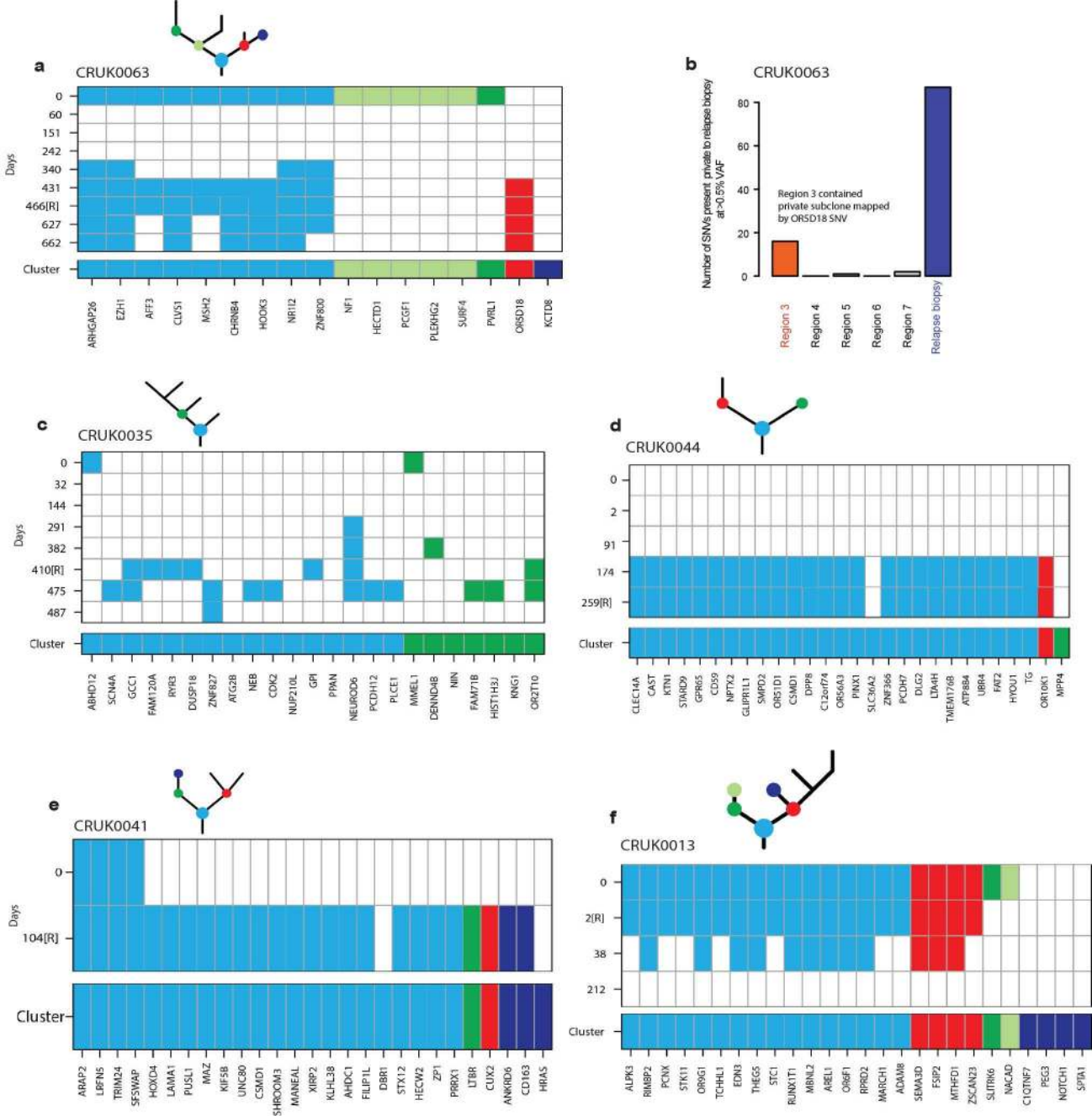
a
CRUK0063
Days
0
60
151
242
340
431
466[R]
627
662
Cluster
ARHGAP26
EZH1
AFF3
CLVS1
MSH2
CHRNB4
HOOK3
NR1I2
ZNF800
NF1
HECTD1
PCGF1
PLEKHG2
SURF4
PVRL1
ORSD18
KCTD8
b
CRUK0063
Number of SNVs present private to relapse biopsy at >0.5% VAF
80
60
40
20
0
Region 3 contained private subclone mapped by ORSD18 SNV
Region 3
Region 4
Region 5
Region 6
Region 7
Relapse biopsy
c
CRUK0035
Days
0
32
144
291
382
410[R]
475
487
Cluster
ABHD12
SCN4A
GCC1
FAM120A
RYR3
DUSP18
ZNF827
ATG2B
NEB
CDK2
NUP210L
GPI
PPAN
NEUROD6
PCDH12
PLCE1
MMEL1
DENND4B
NIN
FAM71B
HIST1H3J
KNG1
OR2T10
d
CRUK0044
0
2
91
174
259[R]
Cluster
CLEC14A
CAST
KTN1
STARD9
GPR65
CD59
NPTX2
GLIPR1L1
SMPD2
OR51D1
CSMD1
DPP8
C12orf74
OR56A3
PINX1
SLC36A2
ZNF366
PCDH7
DLG2
LTA4H
TMEM176B
ATP6B4
UBR4
FAT2
HYOU1
TG
OR10K1
MPP4
e
CRUK0041
Days
0
104[R]
Cluster
ARAP2
LRFN5
TRIM24
SF3WAP
HOXD4
LAMA1
PUSL1
MAZ
KIF5B
UNC80
CSMD1
SHROOM3
MANEAL
XIRP2
KLHL38
AHDC1
FILIP1L
DBR1
STX12
HECW2
ZP1
PRRX1
LTBR
CUX2
ANKRD6
CD163
HRAS
f
CRUK0013
0
2[R]
38
212
Cluster
ALPK3
RIMBP2
PCNX
STK11
OR9G1
TCHHL1
EDN3
THEG5
STC1
RUNX1T1
MBNL2
ARELI
OR6F1
RPRD2
MARCH1
ADAM8
SEMA3D
FSIP2
MTHFD1
ZSCAN23
SLITRK6
NACAD
C1QTNF7
PEG3
NOTCH1
SPTA1

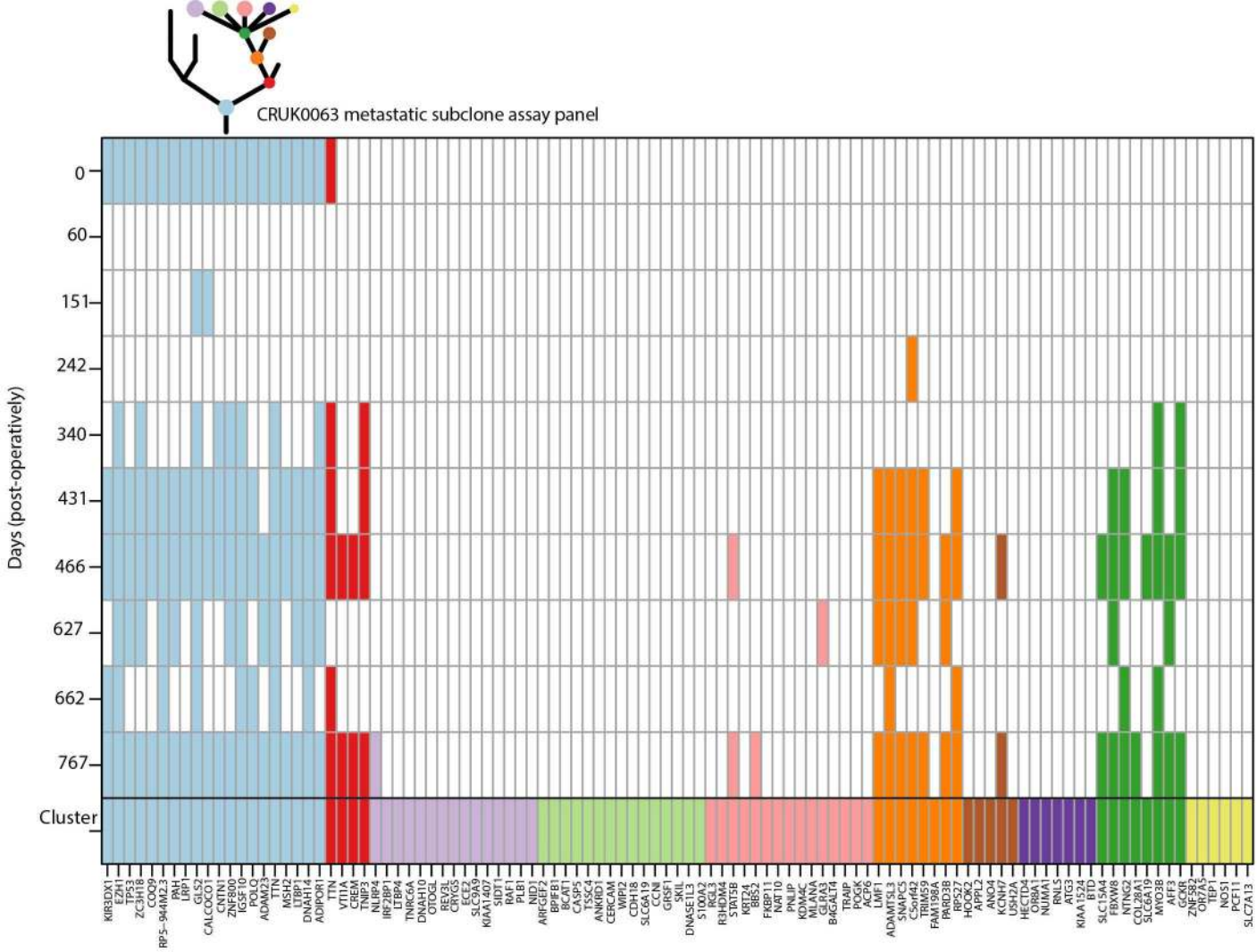
CRUK0063 metastatic subclone assay panel
Days (post-operatively)
0
60
151
242
340
431
466
627
662
767
Cluster
KIR3DX1
EZH1
TP53
ZC3H18
COG9
RP5-944M23.3
IRF1
GLS2
CALCOCO1
CNTN1
ZNF800
IGSF10
POLQ
ADAM23
TTN
MSH3
LTBP1
DNAH14
ADIPOR1
TTN
VTI1A
CREM
TNIP3
NUP54
IRS2
LTBP4
TNRC6A
DNAH10
OTOGL
REV3L
CRYGS
ECE2
SLC30A9
KIAA1407
SIDT1
RAF1
PLB1
NID1
ARFGEF2
BPIFB1
BCAT1
CA5P5
ITGB4
ANKRD10
CERCAM
WIPI2
CDH18
SLC6A19
CCNI
GRSF1
SKIL
DNASE1L3
S100A2
RCL1
R3HDM4
STAT5B
KRT24
BBS2
FKBP11
NAT10
PNLIP
KDM4C
MLANA
GLRA3
B4GALT4
TRAIP
POGK
ACP6
LMF1
ADAMTSL3
SNAPC5
SCN4B
TBX15
FAM198A
PARD3B
RPS27
HOOK2
APPL2
ANO4
KCNH7
ICA1
HECTD4
OR8A1
NUMA1
RNLS
ATG3
KIAA1524
BTD
SLC15A4
FBXW8
NTNG2
COL7A1
SLC6A19
MYO3B
AFF3
GCKR
ZNF382
OR7A5
TP53
NDS1
PCF11
SLC7A13

Extended Table 1 - Patient characteristic tables

a

Clinical characteristics
96 patient pre-operative cohort

Characteristic		Total
Age	<60	19
	≥60	77
Sex	Male	60
	Female	36
ECOG PS	0	49
	1	47
Histology	Adenocarcinoma	58
	Squamous cell carcinoma	31
	Carcinosarcoma	2
	Large cell carcinoma	1
	Adenosquamous carcinoma	3
	Large cell neuroendocrine carcinoma	1
TNM stage	Ia	24
	Ib	35
	IIa	12
	IIb	11
	IIIa	13
	IIIb	1
Lymph node metastasis	Yes	24
	No	72
Pleural involvement	Yes	27
	No	69
Vascular invasion	Yes	41
	No	55
Resection margin	R0	91
	R1	5
Smoking status	Never smoked	11
	Recent ex-smoker	30
	Ex-smoker	48
	Current smoker	7
Ethnicity	White British	85
	White-other	4
	White-Irish	4
	Caribbean	3

b

		No adjuvant therapy	Adjuvant therapy
TNM Stage	Ia	24	0
	Ib	31	4
	IIa	3	9
	IIb	4	7
	IIIa	6	7
	IIIb	0	1

c

Details regarding timing of pre-operative blood sample

Pre-surgery	Number	Details
Less than 24 hours	91	
24-72 hours	2	CRUK0051, 0003
8 days	2	CRUK0073, 0096
31 days	1	CRUK0089

d

Clinical characteristics
24 patient longitudinal sub-cohort

Characteristic		Total
Age	<60	5
	≥60	19
Sex	Male	16
	Female	8
ECOG PS	0	12
	1	12
Histology	Adenocarcinoma	16
	Squamous cell carcinoma	8
TNM stage	Ia	3
	Ib	7
	IIa	3
	IIb	7
	IIIa	3
	IIIb	1
Lymph node metastasis	Yes	9
	No	15
Pleural involvement	Yes	7
	No	17
Vascular invasion	Yes	12
	No	12
Resection margin	R0	23
	R1	1
Smoking status	Never smoked	1
	Recent ex-smoker	5
	Ex-smoker	16
	Current smoker	2
Ethnicity	White British	21
	White-other	2
	Caribbean	1

e

		No adjuvant therapy	Adjuvant therapy
TNM Stage	Ia	3	0
	Ib	6	1
	IIa	0	3
	IIb	2	5
	IIIa	1	2
	IIIb	0	1

Table 2 a - Bespoke panel detected NSCLCs - cross platform validation

Case	Volume cm3	Plasma VAF (mean clonal)	Bespoke-panel ctDNA positive	Histology	Hotspot SNVs tumor	Generic-panel Hotspot SNVs detected
CRUK0029	38.51	2.10	Yes	**LUAD**	1	1
CRUK0009	69.01	1.71	**Yes**	**LUAD**	1	1
CRUK0062	58.48	1.41	**Yes**	**LUSC**	1	1
CRUK0081	16.41	0.21	**Yes**	**LUSC**	1	1
CRUK0089	17.39	0.16	**Yes**	**LUSC**	1	1
CRUK0022	17.20	0.08	**Yes**	**LUAD**	1	0
CRUK0067	6.64	0.07	**Yes**	**LUSC**	1	0
CRUK0052	43.69	0.06	**Yes**	**LUAD**	2	1
CRUK0064	9.24	0.05	**Yes**	**LUSC**	1	0
CRUK0034	10.59	0.01	**Yes**	**LUAD**	1	1

Table 2 b - Bespoke panel non-detected NSCLCs - cross platform validation

Case	Volume cm3	Predicted plasma VAF	Bespoke-panel ctDNA positive	Histology	Hotspot SNVs tumor	Generic-panel Hotspot SNVs detected
CRUK0037	197.42	2.89 (0.93 - 8.97)	No	LUAD	1	0
CRUK0051	27.28	0.30 (0.19 to 0.46)	No	LUAD	1	0
CRUK0004	23.30	0.25 (0.16 to 0.38)	No	LUAD	1	0
CRUK0039	21.68	0.23 (0.15 to 0.35)	No	LUAD	2	0
CRUK0025	19.06	0.20 (0.13 to 0.30)	No	LUAD	2	0
CRUK0014	8.58	0.08 (0.04 to 0.15)	No	LUAD	1	0
CRUK0026	7.45	0.07 (0.04 to 0.13)	No	LUAD	1	0
CRUK0057	5.95	0.05 (0.02 to 0.11)	No	LUAD	1	0
CRUK0018	4.65	0.04 (0.02 to 0.09)	No	LUAD	1	0
CRUK0027	4.61	0.04 (0.02 to 0.09)	No	LUAD	1	0
CRUK0007	4.18	0.04 (0.01 to 0.08)	No	LUAD	1	0
CRUK0049	3.61	0.03 (0.01 to 0.08)	No	LUAD	1	0
CRUK0035	3.31	0.03 (0.01 to 0.07)	No	LUAD	1	0
CRUK0058	2.76	0.02 (0.01 to 0.06)	No	LUAD	1	0
CRUK0021	2.70	0.02 (0.01 to 0.06)	No	LUAD	2	0
CRUK0048	2.16	0.02 (0.01 to 0.05)	No	LUAD	2	0
CRUK0093	0.73	0.004 (0 to 0.03)	No	LUSC	2	0
CRUK0030	0.21	0.001 (0 to 0.01)	No	LUAD	2	0

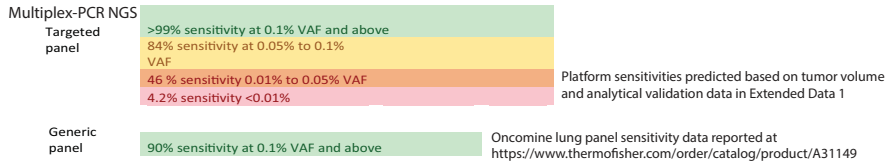

Table 2 c - Variants detected by generic PCR-NGS hotspot panel not detected in M-Seq analysis of tumor

Case	Gene	Location	Position	Ref	Variant	AA change	Plasma VAF	DOR	ctDNA positive	(unfiltered) **Combined exome VAF**	(unfiltered) **Germline VAF**
CRUK0052	**PIK3CA**	chr3	178936091	G	A	p.E545K	0.81	60360	Yes	ND	ND
CRUK0052	**PIK3CA**	chr3	178952085	A	G	p.H1047R	0.12	52325	Yes	0.075	ND
CRUK0062	**PIK3CA**	chr3	178936091	G	A	p.E545K	0.97	89616	Yes	0.016	ND
CRUK0062	**PIK3CA**	chr3	178952085	A	G	p.H1047R	0.05	79205	Yes	0.005	ND
CRUK0062	**TP53**	chr17	7577556	C	A	p.C242F	0.05	93383	Yes	ND	ND
CRUK0089	**TP53**	chr17	7577121	G	A	p.R273C	0.06	59849	Yes	0.168	ND
CRUK0004	**PIK3CA**	chr3	178936091	G	A	p.E545K	0.59	73941	No	0.081	ND
CRUK0018	**PIK3CA**	chr3	178936091	G	A	p.E545K	4.44	99159	No	ND	ND
CRUK0018	**PIK3CA**	chr3	178952085	A	G	p.H1047R	0.81	77806	No	0.044	ND
CRUK0021	**PIK3CA**	chr3	178952085	A	G	p.H1047R	0.11	50107	No	ND	ND
CRUK0027	**PIK3CA**	chr3	178952085	A	G	p.H1047R	0.11	65449	No	ND	ND
CRUK0037	**PIK3CA**	chr3	178952085	A	G	p.H1047R	0.09	51071	No	ND	ND
CRUK0058	**KRAS**	chr12	25398284	C	A	p.G12V	3.44	63090	No	0.124	ND

ND - non detected
DOR - depth of read
Combined exome VAF (unfiltered) - Variant allele frequency across all tumor regions analysed (without call filters).